Scheme 1. Reaction Intermediates and Transition States of the Thermal [4 + 4] Cycloaddition of **4** in the Synthesis of Epoxytwinol A (**1**) As Obtained Using B3LYP/6-31G(d) Calculations

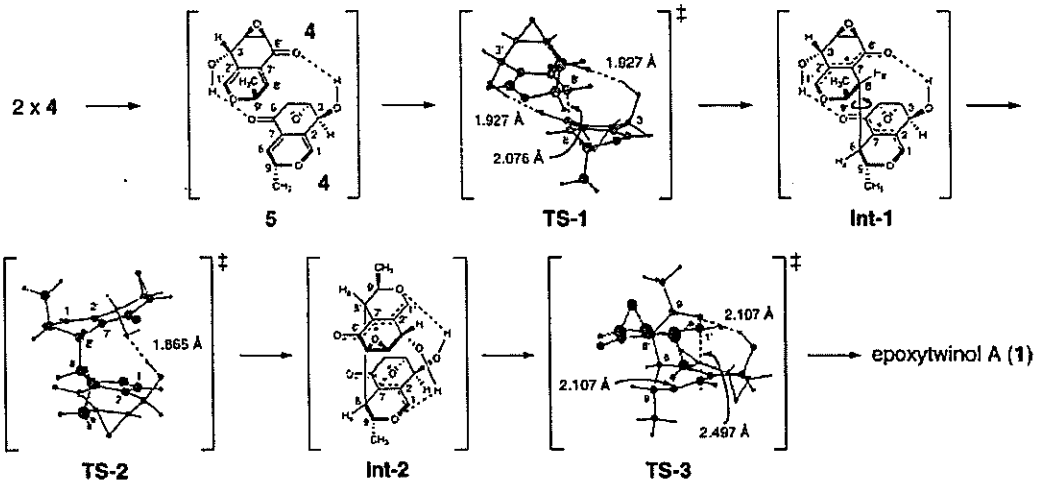

B3LYP (RB3LYP) calculations. A vibrational frequency analysis was carried out on each stationary point.[16] We have confirmed that each stationary point corresponds to a local energy minimum [the number of imaginary frequencies (NImag) = 0], or a transition state [NImag = 1]. In addition, starting from each transition state, an IRC calculation was carried out and the structures of the potential energy minima at both ends of the reaction coordinate were examined. Free energies of the stationary points at 298 K were derived from the B3LYP/6-31G(d) results. These calculations revealed for the first time energy profiles (Figure 2) for the reaction

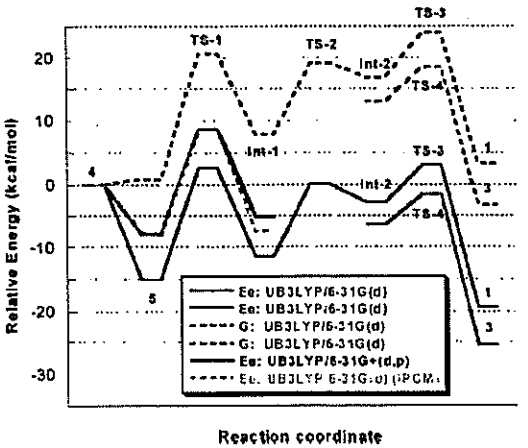

Figure 2. Potential (ee) and free (*G* at 298 K) energy profiles connecting reactant **4**, epoxytwinol A(**1**), and epoxyquinol B (**3**).

pathway of the [4 + 4] cycloaddition reaction. The potential energy profile and the free energy profile both suggest a three-step mechanism involving biradical intermediates (Figure 1). Unless specifically stated, we will refer to the gas-phase UB3LYP/6-31G(d) potential energy differences when discussing relative stabilities of the stationary points in the following sections.

The first process is formation of the C8−C8′ bond. Two monomers **4** preassociate to give complex **5**, which is more stable than two molecules of **4** by 15.1 and 7.9 kcal/mol at the B3LYP/6-31G(d) and B3LYP/6-31+G(d,p) levels, respectively. Counterpoise calculation[17] at these computational levels afforded BSSEs of 7.7 and 2.0 kcal/mol,[18] and hence, the BSSE-corrected stabilization energies for complex **5** are 7.4 and 5.9 kcal/mol.[18] This stabilization can be ascribed to the two hydrogen-bond interactions shown in Scheme 1. From this complex **5**, the C8−C8′ bond is formed affording a biradical intermediate **Int-1** via transition state (**TS-1**), in which there are two hydrogen-bond interactions, and the bond lengths of O- - -H and the forming C8−C8′ bond are 1.927 and 2.076 Å, respectively. Each hydroxy group coordinates to a carbonyl oxygen, acting as a Brønsted acid. In **Int-1**, the dihedral angle Ha-C8−C8′-Ha′ is −171.3°. The barrier height for the first step is 17.6 kcal/mol,[18] and the radical is stabilized by the hydrogen bond interactions.

The second step is rotation about the C8−C8′ bond to afford **Int-2**, in which the dihedral angle Ha-C8−C8′-Ha′ is +26.3°. The transition state (**TS-2**) is shown in Scheme 1, and the activation energy for this second step is 11.5 kcal/mol.[18]

In the third step, an intramolecular radical coupling of **Int-2** generates epoxytwinol A (**1**) with formation of the C1−C1′ bond, the barrier height for this third step being 6.0 kcal/mol.[18] There are also two hydrogen bond interactions in the transition state (**TS-3**), in which the alcohol protons coordinate with a lone pair of the oxygen of the pyran rings and the bond length O- - -H is 2.107 Å.

(16) The "Finegrid" implemented in GAUSSIAN program was employed for the B3LYP calculations and the "Tight" option was applied for geometry optimizations.

(17) Boys, S. F.; Bernardi, F. *Mol Phys.* **1970**, *19*, 553.

(18) See the Supporting Information.

Though there is a possible path leading to **Int-2** directly from **4**, its transition-state energy is higher than that of **TS-1** by 9.8 kcal/mol, indicating that its contribution is negligible.[18]

Furthermore, we have carried out additional calculations for the **reactant**, complex **5**, **TS-1**, and **Int-1**; single-point UB3LYP energy evaluations using the larger basis set 6-31+G(d,p), and UB3LYP/6-31G(d) level solution-phase energy calculations using the isodensity polarizable continuum model (IPCM)[19] with $\epsilon = 2.379$ (toluene is the supposed solvent). It should be noted that using the larger basis set and the IPCM did not alter significantly the above-mentioned gas-phase potential energy profile calculated at the UB3LYP/6-31G(d) level (see Figure 2) and that the calculation is in good agreement with the results of experiments performed in toluene.[10c]

These calculations suggest that the hydroxy group of **4** plays an essential role in this thermal [4 + 4] cycloaddition reaction by forming hydrogen bonds throughout the course of the reaction, from initiation until formation of the final product. The importance of this hydroxy group is supported experimentally by the observations that only Diels–Alder adducts were obtained in the reaction of **6** having no hydroxy or epoxy groups[10d] and in the reaction of **7** containing a methoxy group in place of the hydroxy group[11] (Figure 3).

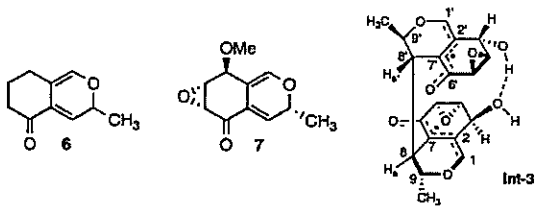

Figure 3. Structures of **6**, **7**, and **Int-3**.

C_2 symmetry is preserved throughout the reaction except at **TS-2**, where the hydrogen bonds recombine. It should be noted that the intermediate radical is rather stable owing to the delocalization of spin density through O1–C1–C2–C7–C6–O2. The spin density of **Int-1**, for example, is shown in Figure 4, which clearly shows the delocalization of the radical.

(19) Foresman, J. B.; Keith, T. A.; Wiberg, K. B.; Snoonian, J.; Frisch, M. J. *J. Phys. Chem.* **1996**, *100*, 16098.

(20) All hydrogens have been omitted for clarity.

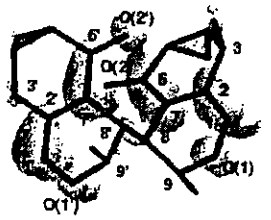

Figure 4. Spin density surface (0.002 electrons/au^3) of **Int-1**.[20]

Calculations indicate that the transformation of epoxytwinol A (**1**) to epoxyquinol B (**3**) also involves three steps. Homolytic cleavage of the C1–C1′ bond affords biradical intermediate **Int-2**. Rotation around the C8–C8′ bond generates **Int-3**, in which the dihedral angle of Ha–C8–C8′–Ha′ is +58.7° (Figure 3). Epoxyquinol B (**3**) is generated by a coupling reaction between C1 and C7′. The transition state energy going from epoxytwinol A (**1**) to epoxyquinol B (**3**) is 22.6 kcal/mol, and the latter is thermodynamically more stable than the former by 6.0 kcal/mol, which explains the facile transformation of the former to the latter.

In summary, we have shown that the [4 + 4] cycloaddition of 2*H*-pyran **4** consists of three consecutive steps involving biradical intermediates. The first step is formation of the C8–C8′ bond with generation of a biradical intermediate (**Int-1**). The next is rotation about the C8–C8′ bond, and the last is radical coupling forming the C1–C1′ bond. The biradicals are stabilized by delocalization, while two hydrogen-bonding interactions are essential for realization of this exceptionally rare thermal [4 + 4] cycloaddition reaction. Biradicals are also involved in the transformation of epoxytwinol A (**1**) into epoxyquinol B (**3**).

Acknowledgment. This work was partially supported by a Grant-in-Aid for Scientific Research on Priority Areas 16073219 from The Ministry of Education, Culture, Sports, Science and Technology (MEXT).

Supporting Information Available: Cartesian coordinates and absolute energies for all reported structures. This material is available free of charge via the Internet at http://pubs.acs.org.

OL052916M

Total Synthesis

DOI: 10.1002/anie.200502826

Concise Enantio- and Diastereoselective Total Syntheses of Fumagillol, RK-805, FR65814, Ovalicin, and 5-Demethylovalicin**

*Junichiro Yamaguchi, Maya Toyoshima, Mitsuru Shoji, Hideaki Kakeya, Hiroyuki Osada, and Yujiro Hayashi**

The inhibition of angiogenesis is a promising method of treating diseases in which this process is involved, such as cancer and rheumatoid arthritis.[1] During our continuing research on angiogenesis inhibitors, we have identified and synthesized several novel compounds with such activity, including epoxyquinols A and B,[2] and azaspirene.[3] Recently, we also isolated RK-805 (**3**) from the fungus *Neosartorya* sp.[4] RK-805 is structurally similar to fumagillin (**1**)[5] and TNP-470 (**2**),[6] a synthetic derivative of fumagillin, which are both inhibitors of angiogenesis. Ovalicin (**6**)[7] is another inhibitor

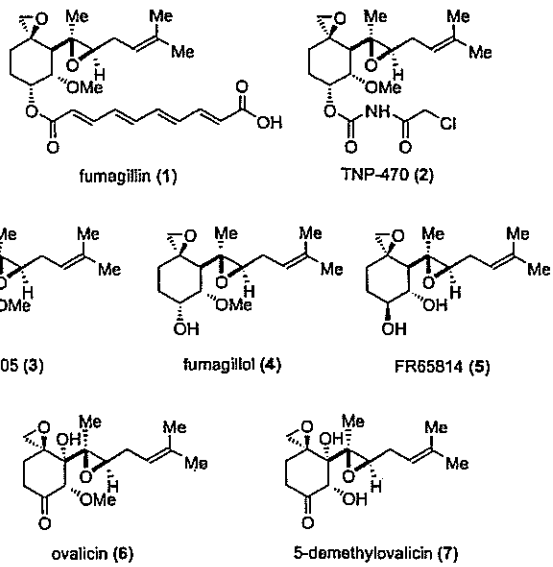

[*] J. Yamaguchi, M. Toyoshima, Dr. M. Shoji, Prof. Dr. Y. Hayashi
Department of Industrial Chemistry
Faculty of Engineering
Tokyo University of Science
Kagurazaka, Shinjuku-ku, Tokyo 162-8601 (Japan)
Fax: (+81) 3-5261-4631
E-mail: hayashi@ci.kagu.tus.ac.jp
Dr. H. Kakeya, Prof. Dr. H. Osada
Antibiotics Laboratory
Discovery Research Institute, RIKEN
Wako, Saitama 351-0198 (Japan)

[**] This paper is dedicated to Prof. E. J. Corey for his elegant total syntheses of the fumagillin and ovalicin families. This work was partially supported by a Grant-in-Aid for Scientific Research on Priority Areas 16073219 from The Ministry of Education, Culture, Sports, Science, and Technology (MEXT).

of angiogenesis and is more stable than fumagillin and TNP-470, while 5-demethylovalicin (**7**)[8] was isolated recently and found to be as potent an angiogenesis inhibitor as ovalicin. While these natural products are anti-angiogenesis agents, FR65814 (**5**),[9] which has a similar structure, displays completely different biological activity and is an immunosuppressant.

Systematic comparison of the biological properties of these natural products and their derivatives is highly desirable.[10] These compounds comprise a cyclohexane framework, two epoxides, and five or six contiguous stereogenic centers, three or four of which are situated on the cyclohexane ring. As a result of their unique structure and important biological properties, they have proved attractive synthetic targets. Four racemic syntheses[11] including Corey's first excellent total syntheses of fumagillin (**1**)[11a] and ovalicin (**6**) have been reported.[11b] The optically active compounds have been prepared from a chiral pool, starting from quinic acid[12] and quebrachitol[13] for ovalicin, glycidol[14] for fumagillin, allose[15] and mannitol[16] for fumagillin, and glucose[17] for FR65814, while diastereoselective syntheses of fumagillin using chiral auxiliaries have been reported by Sorensen[18] and Eustache[19] and their respective co-workers. However, only one catalytic asymmetric synthesis has been reported for any of these compounds, namely, Corey's synthesis of ovalicin (**6**)[20] through substrate-enhanced asymmetric dihydroxylation. Moreover, there is no single, flexible method to access both families. Herein, we disclose the concise, flexible, and highly diastereoselective asymmetric, catalytic total syntheses of compounds of both families, including RK-805 (**3**), fumagillol (**4**), FR65814 (**5**), ovalicin (**6**), and 5-demethylovalicin (**7**) using our recently developed proline-mediated α-aminoxylation of carbonyl compounds[21] as a key step.

Synthesis of the fumagillin family started from 1,4-cyclohexanedione monoethylene ketal (**8**; Scheme 1). α-Aminoxylation of **8** (1.2 equiv) using 10 mol % of L-proline with slow addition of nitrosobenzene (1.0 equiv) over 24 h proceeded efficiently at 0 °C to afford nearly optically pure *R*-α-aminoxylated cyclohexanone **9** (>99% *ee*) in 93% yield, in a reaction that can be scaled up to 25 g of **8** without compromising the yield or enantioselectivity.[21b,c] Reductive cleavage of the N–O bond was performed under an atmosphere of H_2 in the presence of Pd/C[21e] for 3 h in THF (90%). Diastereoselective construction of the epoxide moiety from the ketone carbonyl was found to be troublesome because of easy racemization and low selectivity: Racemic epoxide was obtained, albeit in good yield, when **10** was treated at room temperature with a sulfur ylide such as dimethylsulfonium methylide.[22] The epoxide was generated with low diastereoselectivity (2.5:1–3.4:1) by conventional two-step procedures such as vinylidene formation with $Ph_3P{=}CH_2$ and successive epoxidation with either TBHP in the presence of VO(acac)$_2$[23] at room temperature or MCPBA at 0 °C. After some experimentation, it was found that cyano bis(trimethyl-

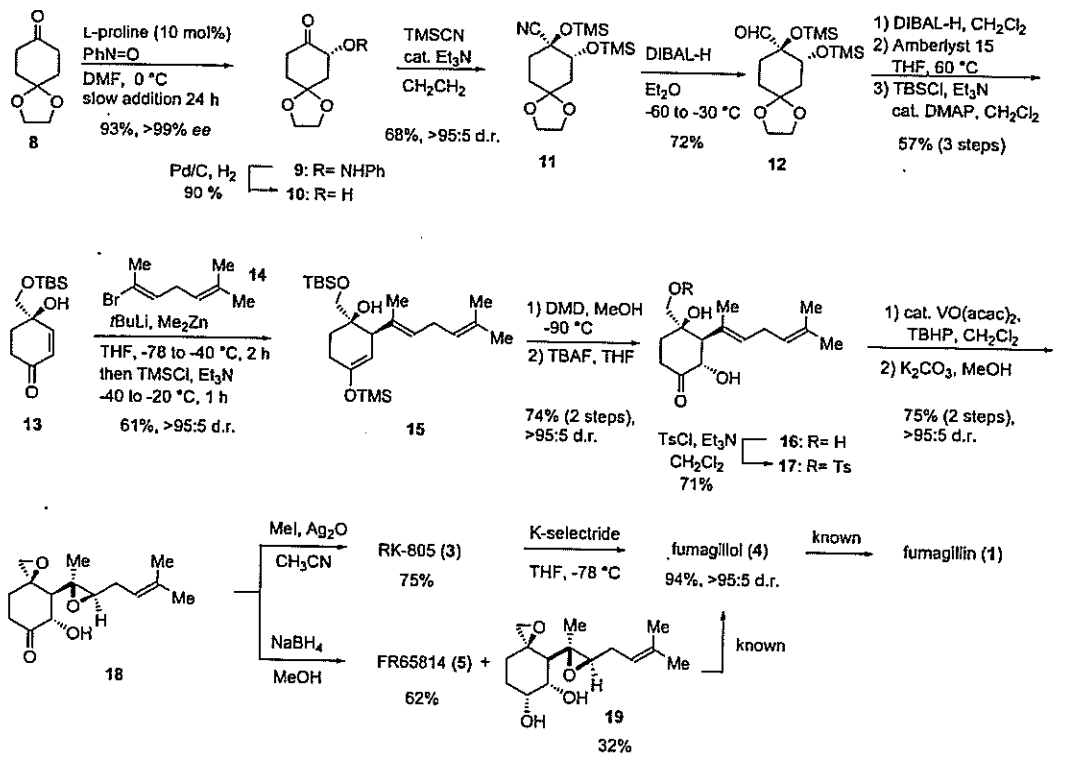

Scheme 1. Total syntheses of fumagillol (**4**), RK-805 (**3**), FR65814 (**5**), and the formal total synthesis of fumagillin (**1**). DMF = *N*,*N*-dimethylformamide; TMS = trimethylsilyl; DIBAL-H = diisobutylaluminum hydride; TBS = *tert*-butyldimethylsilyl; DMAP = 4-(dimethylamino)pyridine; DMD = dimethyldioxirane; TBAF = tetra-*n*-butylammonium fluoride; Ts = *p*-toluenesulfonyl; acac = acetylacetonate; TBHP = *tert*-butylhydroperoxide; selectride = tri-*sec*-butylborohydride.

silyl) ether **11** could be obtained with high diastereoselectivity in moderate yield, although the diastereoselectivity of the initial cyanation was low. When hydroxy ketone **10** was treated with TMSCN (2.5 equiv) in the presence of Et_3N (0.1 equiv)[24] at 0 °C, cyano mono(trimethylsilyl) ethers **20** and **21** were obtained in low diastereoselectivity (3.5:1) after

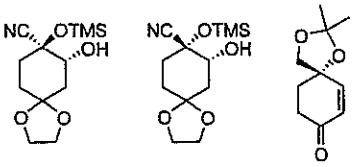

20 **21** **22**

0.5 h. After 2.5 h, however, bis(trimethylsiloxy) cyanocyclohexane **11** was obtained with high diastereoselectivity (> 95:5) in 68 % yield along with cyano mono(trimethylsilyl) ether **21** in 20 % yield because of kinetic discrimination between the diastereomers during the formation of the second TMS ether. The two-step transformation of the cyanide to the alcohol was cleanly performed by repeated reductions with DIBAL-H. Acid treatment with Amberlyst in THF/H_2O at 60 °C for 2 days led to removal of all the protecting groups, with concomitant dehydration affording a cyclohexenone diol. Selective protection of the primary alcohol with TBSCl using Et_3N at room temperature for 12 h afforded TBS ether **13** in 57 % yield over three steps. The optical purity (> 99 % *ee*) of **13** was checked by chiral HPLC analysis of its acetate, which indicated that no racemization had occurred during these transformations. The absolute stereochemistry was confirmed by the conversion of **13** into the enantiomer of Taber's intermediate **22**.[14]

The next task was diastereoselective introduction of the side chain which was also found to be troublesome. The choice of protecting group for the cyclohexenone and the metal cation of the nucleophile are both important for achieving the desired conjugate addition: The tertiary alcohol should be free,[25] and vinyl zincate was found to be the reagent of choice.[26] Thus, α,β-enone **13** reacted with vinyl zincate prepared from **14**[27] at −78 °C to afford the Michael addition product, which was trapped with TMSCl as its trimethylsilyl enol ether **15**. This ether was obtained in 61 % yield as a single isomer, in which the side chain had been introduced stereoselectively from the same side as the hydroxy group. Protection of the tertiary alcohol or use of divinyl cuprate instead of vinyl zincate led to unsatisfactory results. Epoxidation[28] of the silyl enol ether with dimethyldioxirane (DMD) at low temperature (−90 °C) in acetone proceeded diastereoselectively without oxidation of the other trisubstituted double bonds and α-hydroxy cyclohexanone **16** was obtained after treatment with TBAF as a single isomer in 74 % yield over two steps. Though the reaction sequence of conjugate addition, silyl trapping, and Rubottom oxidation was also employed in Taber's synthesis of fumagillin to install a side chain and the hydroxy group at the C5 position, the stereochemistry of the conjugate addition was completely different.[14] Taber et al. reported that intermediate **22** containing an acetal group reacted stereoselectively with a divinyl cuprate derivative in the undesired fashion, that is, *anti* to the oxygen atom of the spirocyclic ether, necessitating several additional steps to correct the stereochemistry. In our synthesis, direct introduction of the side chain with the correct stereochemistry by exploiting the free hydroxy group in combination with a zincate makes the total synthesis efficient and straightforward.

During epoxidation at the side chain, the order of the next two procedures was very important to obtain high diastereoselectivity (Scheme 1). The diastereoselectivity of epoxidation of dihydroxy tosylate **17** with TBHP in the presence of $VO(acac)_2$[23] was excellent, and bis(epoxide) **18** was obtained as a single isomer after treatment with K_2CO_3 in MeOH, whereas reversal of the order of reaction led to low diastereoselectivity (2:1).[29] Formation of the methyl ether with MeI and Ag_2O in CH_3CN gave RK-805, which was stereoselectively reduced with K-selectride at −78 °C to give fumagillol as a single isomer in good yield. The conversion of fumagillol into fumagillin in a single step is known,[11a,14] thus, the formal total synthesis of fumagillin was also accomplished. When **18** was reduced with $NaBH_4$ in MeOH at −50 °C to −10 °C, FR65814 was obtained predominantly in 62 % yield along with **19** in 32 % yield. The conversion of **19** into fumagillol in a single step is known.[11c,18]

Next, the syntheses of 5-demethylovalicin and ovalicin were examined (Scheme 2). The intermediate **12** used in our synthesis of the fumagillin family was employed here also, first to generate the epoxide **24**. Oxidation of **24** with the Dess–Martin periodinane (DMP),[30] followed by acid treatment with thin layer chromatography (TLC) to generate a 3-(2-hydroxyethyloxy)cyclohex-2-enone derivative, and treatment with TBSCl afforded cyclohexenone **25**. The side chain was introduced in a highly diastereoselective manner by using a vinyllithium reagent.[20] As the side chain, the 6-methylhepta-2,5-dien-2-yl substituent was found to be unstable, easy to isomerize, and prone to decomposition, thus its epoxidation had to be carried out immediately.[31] Though conventional epoxidation with $VO(acac)_2$ and TBHP,[23] or *m*-chloroperbenzoic acid gave a complex mixture owing to the instability of the side chain, and the other double bond of the side chain was selectively epoxidized with DMD, $VO(OiPr)_3$[32] was found to be an efficient catalyst, promoting the epoxidation of both the silyl enol ether and the desired side chain alkene at low temperature (−60 °C) to afford 5-demethylovalicin (**7**) as a single isomer with the creation of three chiral centers. The last task necessary to convert 5-demethylovalicin into ovalicin (**6**) was transformation of the alcohol to its methyl ether. Although conventional reagents[33] such as NaH and MeI, Ag_2O and MeI, or MeOTf and 2,6-di-*tert*-butylpyridine, failed, a modification of Corey's method[11b] through the corresponding oxime gave ovalicin stereoselectively. Thus, protection of the alcohol as an ester, formation of the oxime, treatment with base in MeOH, and conversion of the oxime into a ketone gave ovalicin (**6**) as a single isomer, with the ovalicin intermediates **28** and **29** each obtained also as single isomers.[34] Note that oxime **29** was converted into ovalicin (**6**) in good yield without affecting the two epoxides or the trisubstituted alkene under alkylation conditions, when this conversion is usually performed under

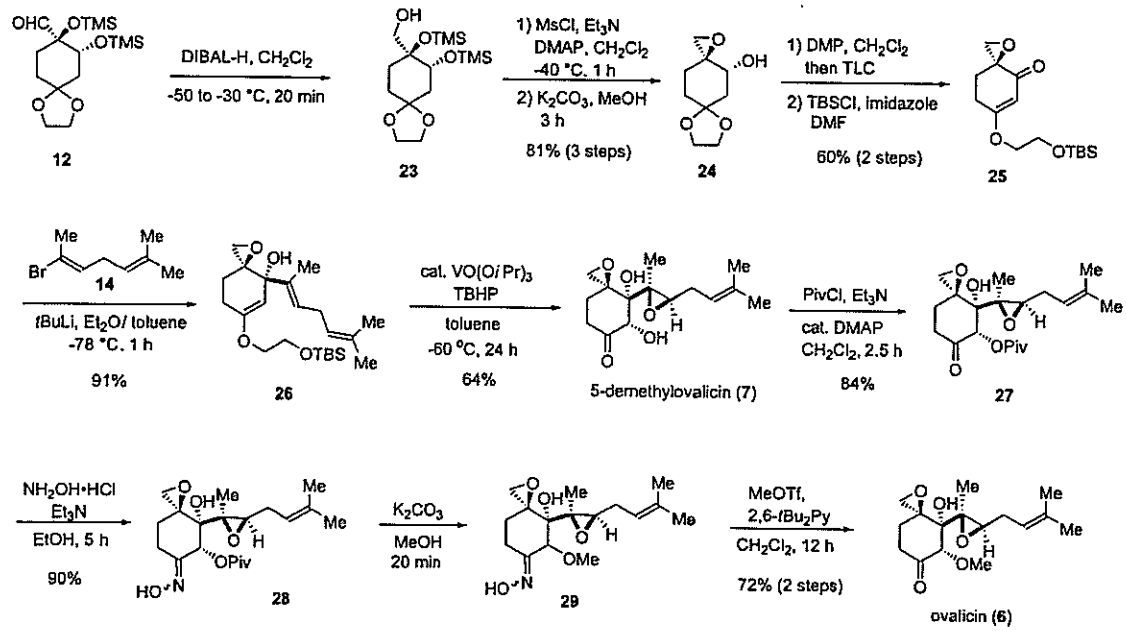

Scheme 2. Total syntheses of ovalicin (**6**) and 5-demethylovalicin (**7**). Ms = methanesulfonyl; DMP = Dess–Martin periodinane; Piv = pivaloyl; OTf = trifluoromethanesulfonate, Py = pyridine.

oxidative, reductive, or acid-hydrolysis conditions.[33] Though the synthetic scheme from **25** is similar to that in Corey's elegant synthesis,[11b] in which introduction of the side chain followed by various functional group manipulations are key transformations, there is an important difference; namely, the effective epoxidation catalyst ($VO(OiPr)_3$), which allows diastereoselective double epoxidation without affecting the labile side chain, saves a couple of steps and improves the efficiency of the synthesis.

The ^1H and ^{13}C NMR spectra, IR spectra, and optical rotations of the synthetic samples of **3**,[4] **4**,[14] **5**,[9] **6**,[13b,35] and **7**[8] are in complete agreement with those previously reported.

In summary, the concise enantio- and diastereoselective total syntheses of fumagillol, RK-805, FR65814, 5-demethylovalicin, and ovalicin in 11–15 steps from commercially available compounds have been demonstrated. These are some of the shortest syntheses reported for these chiral natural products and demonstrate clearly the power of the proline-mediated asymmetric catalytic α-aminoxylation. The initial aminoxylation reaction controls both the absolute and the relative stereochemistry of the subsequently generated stereogenic centers, which are formed by the following transformations: 1) a highly diastereoselective formation of bis(trimethylsilyl ether) cyanide **11** involving kinetic discrimination; 2) a diastereoselective Michael reaction by the use of vinyl zincate (**13**→**15**); 3) a stereoselective double epoxidation catalyzed by $VO(OiPr)_3$ at low temperature (**26**→**7**); and 4) an alkylative deprotection of an oxime (**29**→**6**). Corey's asymmetric total synthesis of ovalicin (**6**)[20] using asymmetric dihydroxylation is a landmark chiral synthesis of a member of the fumagillin and ovalicin families. The present route using an α-aminoxylation catalyzed by inexpensive proline is as efficient as Corey's synthesis;[20] it allows the synthesis to be performed on a large scale and allows easy derivatization, as well as being the first strategy applied to both fumagillin and ovalicin families, thus demonstrating the flexibility of the present synthetic method.

Received: August 9, 2005
Published online: December 20, 2005

Keywords: asymmetric synthesis · inhibitors · natural products · organocatalysis · total synthesis

[1] a) J. Folkman, *J. Natl. Cancer Inst.* **1990**, *82*, 4; b) W. Risau, *Nature* **1997**, *386*, 671; c) M. Klagsbrun, M. A. Moses, *Chem. Biol.* **1999**, *6*, R217; d) G. Gasparini, *Drugs* **1999**, *58*, 17.

[2] a) H. Kakeya, R. Onose, H. Koshino, A. Yoshida, K. Kobayashi, S.-I. Kageyama, H. Osada, *J. Am. Chem. Soc.* **2002**, *124*, 3496; b) H. Kakeya, R. Onose, A. Yoshida, H. Koshino, H. Osada, *J. Antibiot.* **2002**, *55*, 829; c) M. Shoji, J. Yamaguchi, H. Kakeya, H. Osada, Y. Hayashi, *Angew. Chem.* **2002**, *114*, 3324; *Angew. Chem. Int. Ed.* **2002**, *41*, 3192; d) M. Shoji, S. Kishida, M. Takeda, H. Kakeya, H. Osada, Y. Hayashi, *Tetrahedron Lett.* **2002**, *43*, 9155; e) M. Shoji, H. Imai, I. Shiina, H. Kakeya, H. Osada, Y. Hayashi, *J. Org. Chem.* **2004**, *69*, 1548.

[3] a) Y. Asami, H. Kakeya, R. Onose, A. Yoshida, H. Matsuzaki, H. Osada, *Org. Lett.* **2002**, *4*, 2845; b) Y. Hayashi, M. Shoji, J. Yamaguchi, K. Sato, S. Yamaguchi, T. Mukaiyama, K. Sakai, Y. Asami, H. Kakeya, H. Osada, *J. Am. Chem. Soc.* **2002**, *124*, 12078.

[4] Y. Asami, H. Kakeya, R. Onose, Y.-H. Chang, M. Toi, H. Osada, *Tetrahedron* **2004**, *60*, 7085.

[5] M. C. McCowen, M. E. Callender, J. F. Lawlis, *Science* **1951**, *113*, 202.

[6] D. Ingber, T. Fujita, S. Kishimoto, K. Sudo, T. Kanamaru, H. Brem, J. Folkman, *Nature* **1990**, *348*, 555.

[7] H. Sigg, H. P. Weber, *Helv. Chim. Acta* **1968**, *51*, 1395.

[8] K.-H. Son, J.-Y. Kwon, H.-W. Jeong, H.-K. Kim, C.-J. Kim, Y.-H. Chang, J.-D. Choi, B.-M. Kwon, *Bioorg. Med. Chem.* **2002**, *10*, 185.
[9] H. Hatanaka, T. Kino, M. Hashimoto, Y. Tsurumi, A. Kuroda, H. Tanaka, T. Goto, M. Okuhara, *J. Antibiot.* **1988**, *41*, 999.
[10] a) G. Zhou, C. W. Tsai, J. O. Liu, *J. Med. Chem.* **2003**, *46*, 3452; b) V. Rodeschini, J.-G. Boiteau, P. V. de Weghe, C. Tarnus, J. Eustache, *J. Org. Chem.* **2004**, *69*, 357; c) R. Maztischek, A. Huwe, A. Giannis, *Org. Biomol. Chem.* **2005**, *3*, 2150, and references therein.
[11] a) E. J. Corey, B. B. Snider, *J. Am. Chem. Soc.* **1972**, *94*, 2549; b) E. J. Corey, J. P. Dittami, *J. Am. Chem. Soc.* **1985**, *107*, 256; c) D. A. Vosburg, S. Weiler, E. J. Sorensen, *Angew. Chem.* **1999**, *111*, 1022; *Angew. Chem. Int. Ed.* **1999**, *38*, 971; d) M. Hutchings, D. Moffat, N. S. Simpkins, *Synlett* **2001**, *661*.
[12] A. Barco, S. Benetti, C. D. Risi, P. Marchetti, G. P. Pollini, V. Zanirato, *Tetrahedron: Asymmetry* **1998**, *9*, 2857.
[13] a) S. Bath, D. C. Billington, S. D. Gero, B. Quiclet-Sire, M. Samadi, *J. Chem. Soc. Chem. Commun.* **1994**, 1495; b) D. H. R. Barton, S. Bath, D. C. Billington, S. D. Gero, B. Quiclet-Sire, M. Samadi, *J. Chem. Soc. Perkin Trans. 1* **1995**, 1551.
[14] D. F. Taber, T. E. Christos, A. L. Rheingold, I. A. Guzei, *J. Am. Chem. Soc.* **1999**, *121*, 5589.
[15] D. Kim, S. K. Ahn, H. Bae, W. J. Choi, H. S. Kim, *Tetrahedron Lett.* **1997**, *38*, 4437.
[16] O. Bedel, A. Haudrechy, Y. Langlois, *Eur. J. Org. Chem.* **2004**, 3813.
[17] a) S. Amano, N. Ogawa, M. Ohtsuka, S. Ogawa, N. Chida, *Chem. Commun.* **1998**, 1263; b) S. Amano, N. Ogawa, M. Ohtsuka, N. Chida, *Tetrahedron* **1999**, *55*, 2205.
[18] D. A. Vosburg, S. Weiler, E. J. Sorensen, *Chirality* **2003**, *15*, 156.
[19] J.-G. Boiteau, P. Van de Weghe, J. Eustache, *Org. Lett.* **2001**, *3*, 2737.
[20] E. J. Corey, A. Guzman-Perez, M. C. Noe, *J. Am. Chem. Soc.* **1994**, *116*, 12109.
[21] a) Y. Hayashi, J. Yamaguchi, K. Hibino, M. Shoji, *Tetrahedron Lett.* **2003**, *44*, 8293; b) Y. Hayashi, J. Yamaguchi, T. Sumiya, M. Shoji, *Angew. Chem.* **2004**, *116*, 1132; *Angew. Chem. Int. Ed.* **2004**, *43*, 1112; c) Y. Hayashi, J. Yamaguchi, T. Sumiya, K. Hibino, M. Shoji, *J. Org. Chem.* **2004**, *69*, 5966; d) Y. Hayashi, J. Yamaguchi, K. Hibino, T. Sumiya, T. Urushima, M. Shoji, D. Hashizume, H. Koshino, *Adv. Synth. Catal.* **2004**, *346*, 1435; e) G. Zhong, *Angew. Chem.* **2003**, *115*, 4379; *Angew. Chem. Int. Ed.* **2003**, *42*, 4247; f) S. P. Brown, M. P. Brochu, C. J. Sinz, D. W. C. MacMillan, *J. Am. Chem. Soc.* **2003**, *125*, 10808; g) A. Bøgevig, H. Sundeen, A. Córdova, *Angew. Chem.* **2004**, *116*, 1129; *Angew. Chem. Int. Ed.* **2004**, *43*, 1109; h) A. Córdova, H. Sunden, A. Bøgevig, M. Johansson, F. Himo, *Chem. Eur. J.* **2004**, *10*, 3673; i) N. Momiyama, H. Torii, S. Saito, H. Yamamoto, *Proc. Natl. Acad. Sci. USA* **2004**, *101*, 5374; j) W. Wang, J. Wang, H. Li, L. Liao, *Tetrahedron Lett.* **2004**, *45*, 7235; k) H. Sunden, N. Dahlin, I. Ibrahem, H. Adolfsson, A. Córdova, *Tetrahedron Lett.* **2005**, *46*, 3385; for a review, see: l) P. Merino, T. Tejero, *Angew. Chem.* **2004**, *116*, 3055; *Angew. Chem. Int. Ed.* **2004**, *43*, 2995.
[22] E. J. Corey, M. Chaykovsky, *J. Am. Chem. Soc.* **1965**, *87*, 1353.
[23] K. B. Sharpless, R. C. Michaelson, *J. Am. Chem. Soc.* **1973**, *95*, 6136.
[24] S. Kobayashi, Y. Tsuchiya, T. Mukaiyama, *Chem. Lett.* **1991**, 537.
[25] For hydroxy-directed Michael reaction, see: a) K. A. Swiss, D. C. Liotta, C. A. Maryanoff, *J. Am. Chem. Soc.* **1990**, *112*, 9393; b) K. A. Swiss, W. Hinkley, C. A. Maryanoff, D. C. Liotta, *Synthesis* **1992**, 127; c) M. Solomon, W. C. L. Jamison, M. MaCormick, D. Liotta, D. A. Cherry, J. E. Mills, R. D. Shah, J. D. Rodgers, C. A. Maryanoff, *J. Am. Chem. Soc.* **1988**, *110*, 3702.
[26] For Michael reactions of zincate, see: a) M. Suzuki, Y. Morita, H. Koyano, M. Koga, R. Noyori, *Tetrahedron* **1990**, *46*, 4809; b) A. Fürstner, K. Grela, C. Mathes, C. W. Lehmann, *J. Am. Chem. Soc.* **2000**, *122*, 11799.
[27] Vinyl bromide **14** was prepared by Sorensen's modified route[11c,18] of a synthetic procedure originally reported by Corey et al.; see: E. J. Corey, J. Lee, B. E. Roberts, *Tetrahedron Lett.* **1997**, *38*, 8915.
[28] G. M. Rubottom, M. A. Vazquez, D. R. Pellagrina, *Tetrahedron Lett.* **1974**, 4319.
[29] When the spiro epoxide is formed first, the diastereoselectivity of the epoxidation of the side chain is not high. See also reference [11c].
[30] a) D. B. Dess, J. C. Martin, *J. Org. Chem.* **1983**, *48*, 4155; b) D. B. Dess, J. C. Martin, *J. Am. Chem. Soc.* **1991**, *113*, 7277; c) R. E. Ireland, L. Liu, *J. Org. Chem.* **1993**, *58*, 2899.
[31] Epoxidation of the side chain was performed as the last step of Corey's synthesis;[11b] however, we thought it was better to oxidize much earlier owing to the instability of the precursor.
[32] D. R. Pesiri, D. K. Morita, T. Walker, W. Tumas, *Organometallics* **1990**, *18*, 4916.
[33] T. W. Greene, P. G. M. Wuts, *Protective Groups in Organic Synthesis*, 3rd ed., Wiley, New York, **1999**.
[34] The stereochemistry of **28** and **29** was not determined.
[35] D. E. Cane, R. H. Levin, *J. Am. Chem. Soc.* **1975**, *97*, 1282.

PTEN/Akt Signaling through Epidermal Growth Factor Receptor Is Prerequisite for Angiogenesis by Hepatocellular Carcinoma Cells That Is Susceptible to Inhibition by Gefitinib

Shu-ichi Ueda,[1,3] Yuji Basaki,[1,2] Masumi Yoshie,[4] Katsuhiro Ogawa,[4] Shotaro Sakisaka,[3] Michihiko Kuwano,[2,5] and Mayumi Ono[1,2]

[1]Department of Medical Biochemistry, Graduate School of Medical Science and [2]Station-II for Collaborative Research, Kyushu University; [3]Third Department of Medicine, Fukuoka University School of Medicine, Fukuoka, Japan; [4]First Department of Pathology, Asahikawa Medical College, Asahikawa, Japan; and [5]Research Center for Innovative Cancer Therapy of the 21st Century Center of Excellence Program for Medical Science, Kurume University, Kurume, Japan

Abstract

Hepatocellular carcinoma (HCC) is one of the most common tumor-related causes of death worldwide for which there is still no satisfactory treatment. We previously reported the antiangiogenic effect of gefitinib, a selective epidermal growth factor receptor (EGFR) tyrosine kinase inhibitor that has been used successfully to treat lung cancer. In this study, we investigated the effects of gefitinib on tumor-induced angiogenesis by using HCC cell lines (HCC3, CBO12C3, and AD3) *in vitro* as well as *in vivo*. Oral administration of gefitinib inhibited angiogenesis induced by HCC3 and CBO12C3, but not by AD3 in the mouse dorsal air sac model. Production of both vascular endothelial growth factor (VEGF) and chemokine C-X-C motif ligand 1 (CXCL1) by EGF-stimulated HCC was more markedly inhibited by gefitinib in HCC3 and CBO12C3 cells than in AD3 cells. EGF stimulated the phosphorylation of EGFR, Akt, and extracellular signal-regulated kinase 1/2 (ERK1/2) in HCC3 and CBO12C3 cells, whereas EGF stimulated phosphorylation of EGFR and ERK1/2, but not Akt in AD3 cells. In fact, Akt was constitutively activated in the absence of EGF in AD3 cells. Gefitinib inhibited Akt phosphorylation in all three cell lines, but it was about five times less effective in AD3 cells. The concentration of PTEN in AD3 cells was about a half that in HCC3 and CBO12C3 cells. Transfection of HCC3 cells with PTEN small interfering RNA reduced their sensitivity to gefitinib in terms of its inhibitory effect on both Akt phosphorylation and the production of VEGF and CXCL1. In conclusion, effect of gefitinib on HCC-induced angiogenesis depends on its inhibition of the production of angiogenic factors, probably involving a PTEN/Akt signaling pathway. (Cancer Res 2006; 66(10): 5346-53)

Introduction

Hepatocellular carcinoma (HCC) is the fifth most common malignancy worldwide (1) and the prognosis for HCC patients is still very poor. Members of the epidermal growth factor receptor (EGFR) family have emerged as critical factors in the development and growth of various types of cancer, including HCC (2). These receptors are part of a complex network of signal transduction cascades that modulate tumorigenic processes, such as proliferation, adhesion, migration, differentiation, angiogenesis, and escape from apoptosis (3–6). High EGFR expression in human cancers is often correlated with advanced disease, metastasis, and poor clinical outcome, for example in non–small cell lung carcinoma (NSCLC), breast, cervical, and head and neck carcinomas (7–9).

Gefitinib (Iressa, ZD1839) is an orally active and selective EGFR tyrosine kinase inhibitor that blocks EGFR-mediated signal transduction pathways involved in cancer growth (10, 11). Gefitinib has antiproliferative activity in various human cancers *in vivo* as well as *in vitro* (12, 13). It is now approved as a monotherapy for patients with locally advanced or metastatic NSCLC (14–16) and is under investigation for the treatment of prostate, breast, head and neck, gastric, and colorectal cancer (17). An important recent discovery is the close association between a clinical response to gefitinib in patients with NSCLC and somatic mutations in the *EGFR* gene (18, 19). In NSCLC cells carrying such mutations, gefitinib treatment markedly inhibited phosphorylation of EGFR and its downstream signaling kinases, Akt and extracellular signal-regulated kinase 1/2 (ERK1/2). Consistent with this observation, we have reported that the sensitivity of NSCLC cell lines to gefitinib under basal growth condition is closely correlated with their dependence for survival and proliferation on Akt and ERK1/2 activation in response to EGFR signaling (20). Cappuzzo et al. (21) have reported that patients with phosphorylated Akt–positive tumors who received gefitinib had a better response rate and time to progression. Moreover, increased *EGFR* gene copy number evaluated by fluorescent *in situ* hybridization (FISH) was significantly associated with higher response rates and lower progression rates in lung cancer (22) and in colon cancer (23).

HCC is a typical hypervascular tumor and tumor angiogenesis is a prerequisite for both its growth and metastasis (24, 25). Angiogenesis and vascular invasion are common characteristics of malignant tumors in patients with HCC (26, 27). Enhanced expression of vascular endothelial growth factor (VEGF) and chemokine C-X-C motif ligand 1 (CXCL1) is often seen both in HCC cells in culture and at sites of angiogenesis in the livers of HCC patients (26, 28–33). Ishikawa et al. (34) have previously reported antitumor effect by antiangiogenesis gene therapy using *angiostatin* gene on HCCs in the xenograft model. A recent study by Liu et al. (35) has also shown that administration of a VEGFR tyrosine kinase inhibitor induced both antitumor and antiangiogenesis effects against HCCs in the xenograft model. On the other hand, we have previously reported the inhibition of EGF-induced migration of vascular endothelial cell and neovascularization in mouse corneas by gefitinib, suggesting that its antitumor effect

Requests for reprints: Mayumi Ono, Department of Medical Biochemistry, Graduate School of Medical Sciences, Kyushu University, 3-1-1 Maidashi Higashi-ku, 812-8582 Fukuoka, Japan. Phone: 81-92-642-6098; Fax: 81-92-642-6203; E-mail: mayumi@biochem1.med.kyushu-u.ac.jp.

doi:10.1158/0008-5472.CAN-05-3684

may be mediated in part through its antiangiogenic activity (36, 37). Overexpression of EGFR was also observed in 60% to 85% of tumor tissue of HCC (38), and a phase II trial of gefitinib has been proceeding against patients with advanced unresectable HCC in the United States. In this study, we asked whether EGFR inhibition could modulate tumor angiogenesis induced by HCC cells and examined possible mechanisms underlying the effects of gefitinib.

Materials and Methods

Cell culture and reagents. Three murine HCC cell lines HCC3, CBO12C3, and AD3 were established as described previously (39, 40) and were cultured in William's E (Life Technologies, Inc., Grand Island, NY) supplemented with 10 ng/mL EGF, 10% fetal bovine serum (FBS), 320 mg/L L-glutamine, and 2 g/L glucose, at 37°C in 5% CO_2 in a humid environment. Gefitinib was provided by Astra Zeneca Pharmaceuticals (Macclesfield, United Kingdom) and was dissolved in DMSO for *in vitro* studies as described previously (20, 27). LY294002, a selective inhibitor of phosphatidylinositol 3-kinase (PI3K), and U0126, an ERK inhibitor, were purchased from Sigma Chemical Co. (St. Louis, MO). Recombinant EGF, anti-phospho-EGFR (Tyr^{1173}), anti-EGFR, and anti-PI3K p85 antibodies were purchased from Upstate Biotechnology, Inc. (Lake Placid, NY). Anti-phospho-Akt (Ser^{473}), anti-Akt, anti-phospho-ERK1/2 (Thr^{202}/Tyr^{204}), and anti-ERK1/2 antibodies were purchased from Cell Signaling Technology (Beverly, MA). Anti-PTEN and anti-PI3K p110 antibodies were from Santa Cruz Biotechnology, Inc. (Santa Cruz, CA). Anti-β-actin antibody was from Abcam, Ltd. (Cambridge, United Kingdom).

Cell proliferation assay. HCC cells were suspended at 5.0×10^3/mL in medium with or without 10 ng/mL EGF and seeded into 48-well plates for the indicated periods. The following day, cell numbers were counted using a Z1 Series Coulter Counter (Beckman Coulter, Inc., Fullerton, CA).

Mouse dorsal air sac assay. This assay was carried out in 7- to 10-week-old male mice as previously described (41). Male BALB/c mice were obtained from Kyudo Co., Ltd. (Fukuoka, Japan). HCC cells (2×10^6) were suspended in 150 μL PBS and injected into a chamber that consisted of a ring (Millipore Corp., Bedford, MA) covered with Millipore filters (0.45 μm pore size) on each side. This was implanted into an air sac produced by injecting 10 mL of air s.c. on the back of an anesthetized mouse (50 mg/kg pentobarbital, i.v.) on day 0. Gefitinib was administered p.o. from day 0 to day 4. On day 5, the chambers were removed from the s.c. fascia and replaced with black rings of the same inner diameter as the chambers. Photographs of these sites were assessed by counting the number of newly formed vessels >3 mm in length within the area of the rings.

Quantification of VEGF and CXCL1 in conditioned medium. The concentrations of VEGF and CXCL1 in conditioned medium from HCC cells were measured using ELISA kits (R&D Systems, Minneapolis, MN) as described previously (42). Briefly, HCC cells were seeded in 24-well dishes at 2.5×10^4/2 mL/well and, when subconfluent, the medium was replaced with serum-free medium for 24 hours, containing different concentrations of kinase inhibitors, with or without 10 ng/mL EGF at 37°C. Results are presented as means ± SD.

Western blot analysis. After culture for 12 hours in serum-free medium without EGF, HCC cells were treated with the indicated concentration of gefitinib for 3 hours and then stimulated with 10 ng/mL EGF for 15 minutes at 37°C. After rinsing with ice-cold PBS, the cells were lysed in Triton X-100 buffer [50 μmol/L HEPES (pH 7.4), 150 mmol/L NaCl, 1% Triton X-100, 10% glycerol, 1 mmol/L phenylmethylsulfonyl fluoride, 10 μg/mL aprotinin, 10 μg/mL leupeptin, and 1 mmol/L Na_3VO_4]. Lysates were subjected to SDS-PAGE and transferred to Immobilon membranes (Millipore). Blots were incubated with primary antibodies and visualized with a secondary antibody coupled to horseradish peroxidase (Amersham, Piscataway, NJ), and enhanced chemiluminescence system, as described previously (20). Bands on Western blots were analyzed densitometrically using Scion Image software (version 4.0.2; Scion Corp., Frederick, MD).

PTEN gene silencing using small interfering RNA. The ability of 25-nucleotide duplexes of RNA to interfere with PTEN expression was tested. The specific small interfering RNA (siRNA) sequence used was nucleotide 58 to 82, relative to the first nucleotide of the start codon, of PTEN (Genbank accession number NM_008960). Mock siRNA duplexes were obtained from Invitrogen (Carlsbad, CA). siRNA duplexes were transfected using LipofectAMINE 2000 and Opti-MEM medium (Invitrogen) according to the recommendations of the manufacturer. Reduction in PTEN expression was confirmed by Western blot analysis.

FISH analysis. FISH analysis was done as described previously (43). Mouse EGFR cDNA (BC-023729-EGFR) and Mere Mouse BAC clone 43L24 were obtained from Open Biosystems (Huntsville, AL). The probes for EGFR and chromosome 11 were labeled with digoxigenin and biotin by nick translation methods, respectively. The slides were incubated at 75°C for 10 minutes to codenature the EGFR and chromosome 11 probes and allowed to hybridize overnight at 37°C. After stringency wash, digoxigenin-labeled EGFR and biotin-labeled chromosome 11 probes were detected using antidigoxigenin-Cy3 and anti-biotin-Cy5. The chromatin was counterstained with 4′,6-diamino-2-phenylindole. Analysis was done with a Leica DMRA2 fluorescence microscope (Deerfield, IL) equipped with the Leica CW4000 FISH software. Average numbers of chromosome were determined by scoring 30 to 40 metaphase spreads.

Statistical analysis. Statistical analysis used the Mann-Whitney *U* test and Student's *t* test, with $P < 0.05$ considered statistically significant, and was done using JMP 5.01 software (SAS Institute, Inc. Cary, NC).

Results

Effect of EGF on the cell growth of HCC cell lines. The growth rates of HCC cell lines were measured under normal growth conditions with 10% FBS, in the presence or absence of 10 ng/mL EGF. Doubling times for HCC3, CBO12C3, and AD3 were 13.5, 12.1, and 12.6 hours, respectively, in the presence of EGF and 22.4, 14.6, and 14.6 hours, respectively, in the absence of EGF (Fig. 1). Growth rates for the three lines were comparable, although EGF affected the growth of HCC3 cells rather more than that of the other two cell lines.

Gefitinib inhibits tumor-induced angiogenesis *in vivo*. We next investigated whether gefitinib could inhibit angiogenesis induced by HCC cells *in vivo*, using the dorsal air sac assay. In the absence of gefitinib, implantation of chambers containing each of the three HCC cell lines resulted in the development of microvessels with thin curled structures and tiny bleeding spots, in addition to the preexisting vessels (Fig. 2*A*), consistent with our previous studies (41). The oral administration of gefitinib at 150 mg/kg/d markedly reduced the development of microvessels induced by HCC3 and CBO12C3 cells, but not by AD3 cells (Fig. 2*A*). About a 60% reduction in angiogenesis was seen in mice implanted with HCC3 cells and given 75 mg/kg/d gefitinib and a similar reduction was seen in mice implanted with CBO12C3 cells and given 150 mg/kg/d gefitinib (Fig. 2*B*).

Inhibitory effect of gefitinib on production of VEGF and CXCL1 in HCC cells. To understand how gefitinib modulates angiogenesis, we examined the effect of this EGFR-selective drug on the production of two potent inducers of angiogenesis, VEGF and CXCL1 [interleukin-8 (IL-8) homologue/KC/Gro-α] in HCC cell lines (Fig. 3*A*). EGF increased the production of both VEGF and CXCL1 by 1.6- to 3.2-fold in all three cell lines. At 0.1 to 5.0 μmol/L, gefitinib inhibited EGF-stimulated production of VEGF and CXCL1 by HCC3, CBO12C3, and AD3 to different extents. At 1 μmol/L, gefitinib blocked the production of CXCL1 by >80% in HCC3 and CBO12C3 cells and by 60% in AD3 cells in the presence of EGF. At the same concentration, gefitinib also blocked VEGF production by

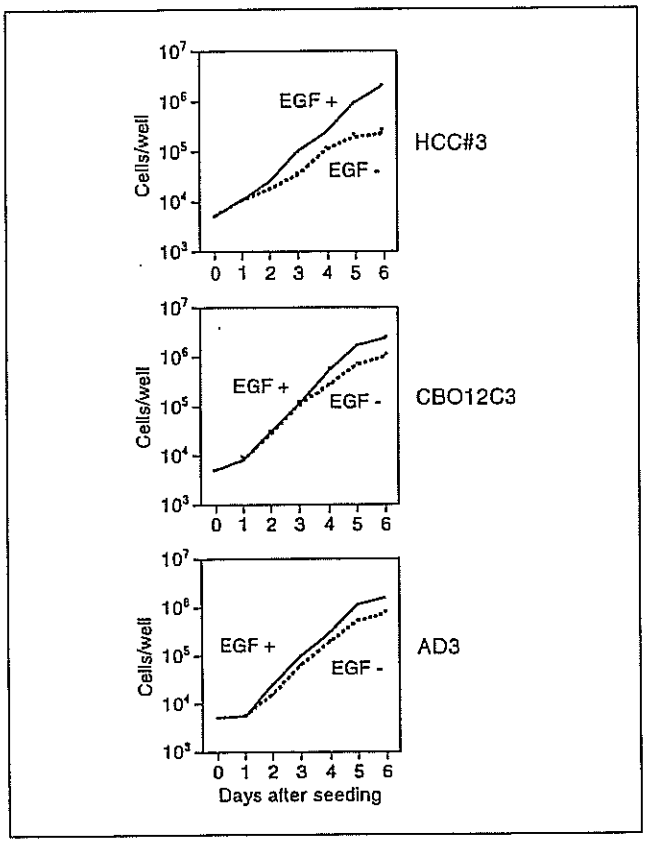

Figure 1. Effect of EGF on the cell growth of three HCC cell lines, HCC3, CBO12C3, and AD3: 5.0 × 10^3/well were incubated with or without 10 ng/mL EGF in 48-well plates. The cells were counted at the times indicated. *Points*, mean of triplicate wells; *bars*, SD.

HCC3 and CBO12C3 cells by 60% to 80%, whereas VEGF production by AD3 cells was only inhibited by 20% in the presence of EGF (Fig. 3*A*). The production of VEGF and CXCL1 in response to exogenous EGF was rather more sensitive to inhibition by gefitinib in HCC3 and CBO12C3 cells compared with AD3 cells.

Effect of gefitinib on phosphorylation of EGFR, Akt, and ERK1/2 in HCC cells. When EGFR binds EGF or transforming growth factor-α, it is autophosphorylated and activates a number of downstream signaling molecules, such as Akt and mitogen-activated protein kinase (ERK1/2; ref. 42). We examined the effect of gefitinib on the phosphorylation of EGFR, Akt, and ERK1/2 in the three cell lines *in vitro*. Exogenous EGF enhanced the phosphorylation of EGFR, Akt, and ERK1/2 in HCC3 and CBO12C3 cells. By contrast, EGF enhanced the phosphorylation of EGFR and ERK1/2, but not Akt, in AD3 cells; Akt was constitutively phosphorylated in AD3 cells when EGF was added exogenously (Fig. 3*B*). Phosphorylation of Akt was also inhibited by gefitinib to different extents in the three cell lines: 0.1 μmol/L gefitinib inhibited Akt phosphorylation in HCC3 and CBO12C3 by 50% compared with EGF alone, but had no effect at this concentration in AD3 cells (Fig. 3*B*). Although Akt was constitutively phosphorylated in the absence of EGF in AD3 cells, phospho-Akt was rather less sensitive to the inhibitory effect of gefitinib in AD3 than in the other two cell lines.

Involvement of Akt and ERK1/2 in EGF-induced production of angiogenic factors, VEGF and CXCL1. To identify the EGF/EGFR-activated signal pathways involved in the production of angiogenic factors, we looked at the effects of LY294002, a selective inhibitor of PI3K, and U0126, an inhibitor of ERK1/2, on the production of VEGF and CXCL1 by HCC3 and AD3 cells. LY294002 inhibits Akt activation by specifically blocking PI3K, a positive regulator of Akt kinase. EGF increased VEGF and CXCL1 production in both these cell lines 2- to 3-fold (see Fig. 3*A*) and treatment with LY294002 resulted in a significant decrease in the production of both factors in HCC3 cells compared with EGF alone (Fig. 4*A* and *B*). However, LY294002, tested up to a concentration of 5 μmol/L, had no effect on the EGF-induced production of VEGF and CXCL1 in AD3 cells (Fig. 4*A* and *B*). Treatment with U0126 also affected cellular production of VEGF in both cell lines but there was no significant difference in the inhibitory effect of U0126 on cellular production of VEGF between two cell lines (Fig. 4*C*). U0126 showed only a slight, if any, inhibition of CXCL1 production, but there was no significant difference in its inhibition between two cell lines (Fig. 4*D*).

Role of PTEN in gefitinib-mediated inhibition of Akt activation and production of angiogenic factors. Akt activation is regulated by both phosphorylation at serine-473 and PIP_3

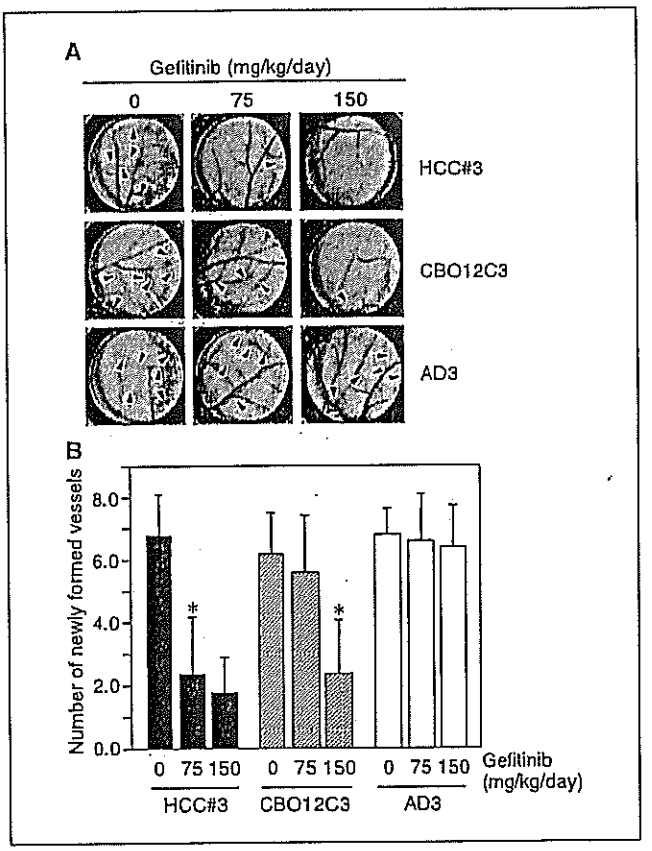

Figure 2. Effect of gefitinib on angiogenesis induced by HCC cell lines in the mouse dorsal air sac assay. *A*, representative photographs of assay chambers containing HCC3, CBO12C3, or AD3 cells, with or without gefitinib at 75 or 150 mg/kg/d. *Arrowhead*, newly formed vessels, with characteristic zigzagging lines. Gefitinib was given p.o., daily, for 5 days. *B*, quantitative analysis of tumor angiogenesis induced by three HCC cell lines and its inhibition by gefitinib. The angiogenic responses were determined by counting the number of new blood vessels >3 mm in length as shown in (*A*). *Columns*, mean of five or six mice; *bars*, SD. *, $P < 0.05$; **, $P < 0.01$ compared with controls using the two-tailed Mann-Whitney *U* test.

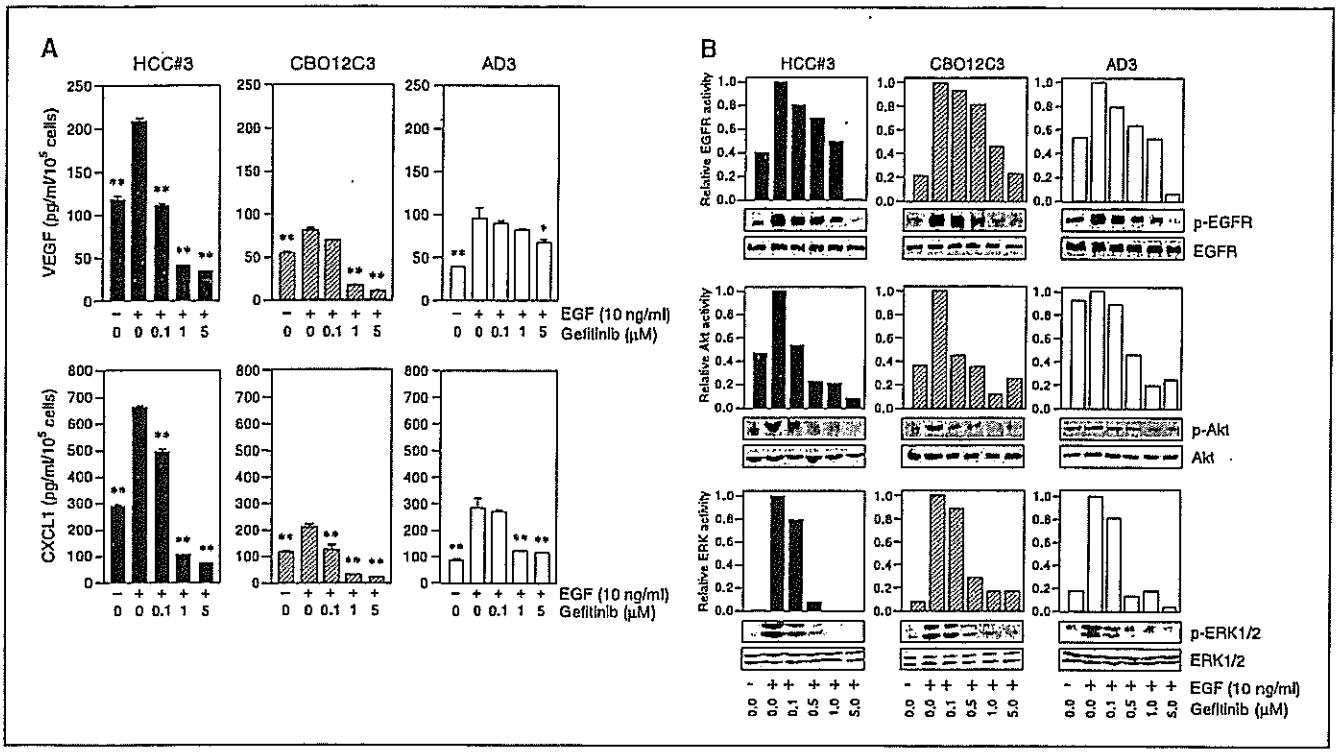

Figure 3. Effect of gefitinib on the EGF-induced production of angiogenic factors and phosphorylation of EGFR, Akt, and ERK1/2 in HCC cell lines. *A*, 2.5×10^4 cells per well were incubated in the presence or absence of 10 ng/mL EGF, with or without different doses of gefitinib, in 24-well plates for 24 hours. VEGF and CXCL1 were measured in culture supernatants with an ELISA kit. *Columns*, mean for triplicate wells; *bars*, SD. *, $P < 0.05$; **, $P < 0.01$ compared with treatment with EGF alone using the two-tailed Student's *t* test. *B*, the cells were stimulated with 10 ng/mL EGF for 15 minutes with or without gefitinib at the concentrations indicated. Protein extracts were resolved by Western blot analysis and probed with various antibodies. Activities of phosphorylated EGFR, Akt, and ERK1/2 were normalized to their nonphosphorylated form when each activity of phospho-EGFR, phospho-Akt, and phospho-ERK1/2 in the presence of EGF without gefitinib in three cell lines was normalized as 1.0.

binding to pleckstrin homology domain of Akt. The level of cellular PIP_3 is controlled by PI3K and the lipid phosphatase, PTEN (44). We compared the expression of PI3K and PTEN in the three cell lines in the presence or absence of EGF. In the absence of EGF, all three cell lines expressed similar levels of the PI3K catalytic subunit, p110, but HCC3 and CBO12C3 expressed rather higher levels of the regulatory subunit, p85, than AD3 (Fig. 5*A*). Quantitative analysis showed that PTEN was expressed in AD3 at about half the level in HCC3 or CBO12C3, both in the absence and presence of EGF (Fig. 5*A*). This difference in PTEN expression between AD3 and the other two cell lines was consistently found in repeated experiments with independently cultured cell lines (data not shown).

Because gefitinib had been found to be a much less effective inhibitor of Akt activation and angiogenic factor production in AD3 cells than in HCC3 cells (Fig. 3*B*), we next examined whether the lower expression of PTEN in AD3 could be related to this. In HCC3 cells transfected with PTEN siRNA, the *PTEN* gene was very effectively silenced (see Fig. 5*B*); Akt was found to be phosphorylated in the absence of EGF, but was not in mock-transfected cells; and Akt phosphorylation was much less sensitive to inhibition by gefitinib (Fig. 5*C*). We then looked at cellular levels of CXCL1 and VEGF. The cellular levels of CXCL1, but not VEGF, in PTEN siRNA-transfected HCC3 cells were about half those in mock-transfected cells (Fig. 5*D*) and the production of both VEGF and CXCL1 in response to EGF became insensitive to inhibition by gefitinib.

Increased *EGFR* gene copy number in HCC cells. Cappuzzo et al. (22) reported that gene amplification and copy number of *EGFR* gene in association with Akt activation is closely associated with drug sensitivity on therapeutic efficacies of gefitinib in NSCLC. We examined if *EGFR* gene was amplified in liver cancer cell lines, HCC3 and AD3 by FISH analysis. HCC3 and AD3 cells showed increased copy number of *EGFR* gene compared with normal spleen cells (Fig. 6). However, *EGFR* gene amplification was not observed in both HCC3 and AD3. HCC3 cells were near triploid with 2.7 ± 0.9 copies of chromosome 11 per cells and 61.3 ± 18.4 of chromosome per cells. AD3 cells were near tetraploid with 3.7 ± 0.9 copies of chromosome 11 per cells and 77.8 ± 18.3 of chromosome per cells. We found that both cell lines increased copy number of *EGFR* gene; however, there was no apparent difference in both gene amplification and copy number of EGFR in HCC3 and AD3.

Discussion

We have previously reported that gefitinib inhibits EGF-induced angiogenesis both *in vitro* and *in vivo* (36, 37). In this study, we have shown for the first time that tumor-induced angiogenesis in the mouse dorsal air sac assay can be blocked by gefitinib treatment. However, when different HCC cell lines were used in this model to induce angiogenesis, its susceptibility to inhibition by this drug was found to vary. Angiogenesis induced by HCC3 cells was most susceptible to inhibition by gefitinib. Angiogenesis induced by

CBO12C3 cells was also inhibited by gefitinib, but at higher doses of the drug. In contrast, angiogenesis induced by AD3 was relatively resistant to inhibition by gefitinib.

We first examined expression of which angiogenic factor was augmented by exogenous addition of EGF in HCC cell lines by membrane-bound antibody array technology. Of various angiogenesis-related factors, we observed up-regulation of *VEGF* and *CXCL1* genes by EGF (data not shown), and we focused on these two potent angiogenic factors. In all HCC lines, EGF was found to enhance cellular production of both VEGF and CXCL1. The production of these potent angiogenic factors was also more effectively inhibited by gefitinib in HCC3 and CBO12C3 cells than that in AD3 cells. This suggests that the inhibitory effect of gefitinib on HCC-induced angiogenesis might be due to its effect on the production of such angiogenic factors. The production of angiogenic factors, including VEGF and IL-8, is often enhanced by EGF, TGF-α, and other cytokines in tumor cell lines (25, 38, 45–48). Consistent with these previous studies, the production of both VEGF and CXCL1 increased 1.6- to 3.2-fold with EGF treatment in all three HCC cell lines. The fact that gefitinib was a much less effective inhibitor of VEGF and CXCL1 production in AD3 than in HCC3 and CBO12C3 cells suggests that the EGF induction mechanism in AD3 cells may be refractory to gefitinib. Our previous studies suggested two pathways by which gefitinib could exert its antiangiogenic effects: (*a*) EGF/TGF-α up-regulates the expression of angiogenic factors by cancer cells themselves, resulting in the induction of angiogenesis by a paracrine mechanism, and this process is inhibited by gefitinib; or (*b*) EGF/TGF-α induces angiogenesis through direct interaction with EGFRs on endothelial cells and this process is inhibited by gefitinib (36, 37). In our studies of EGF-induced neovascularization in the mouse cornea, we obtained evidence supporting the latter pathway as gefitinib inhibited activation of EGFR in the new vessels themselves (37). The results of our present study suggest that the former pathway is a more likely candidate because gefitinib inhibited the production of both VEGF and CXCL1 by HCC cells.

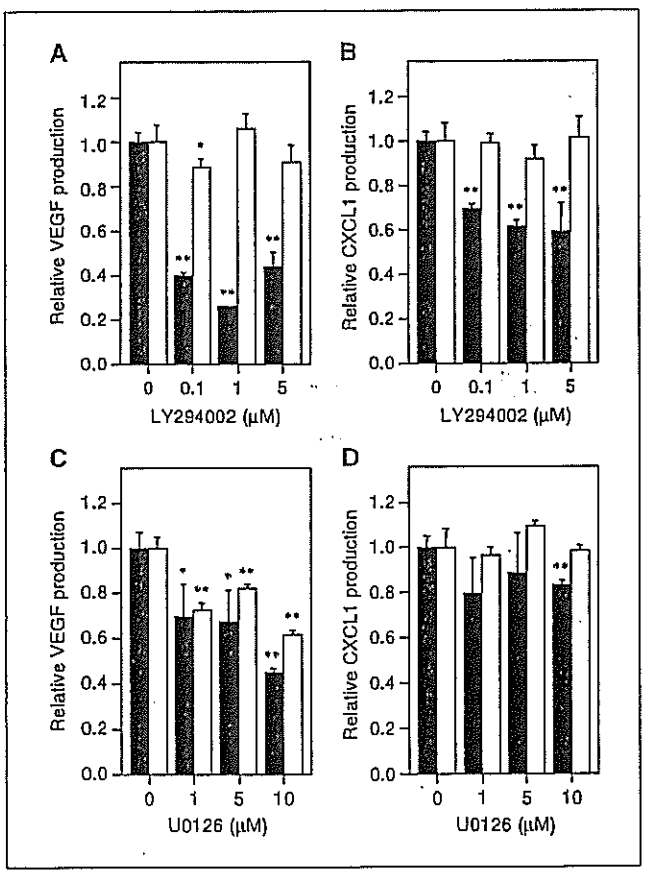

Figure 4. Effect of kinase inhibitors, LY294002 and U0126, on the production of VEGF and CXCL1 by HCC3 and AD3 cells cultured in the presence of EGF. Cells (2.5×10^4/well) were incubated with or without kinase inhibitors in 24-well plates for 24 hours. VEGF and CXCL1 were measured in culture supernatants using ELISA kits. Concentrations of the angiogenic factors in the presence of inhibitors were normalized to those in the absence of inhibitors. *Columns*, mean of triplicate wells for HCC3 (*closed*) and AD3 (*open*); *bars*, SD. *, $P < 0.05$; **, $P < 0.01$ compared with treatment with EGF alone using the two-tailed Student's *t* test.

While studying the mechanism underlying the different inhibitory effects of gefitinib on VEGF and CXCL1 production by HCC cell lines, we found that the drug had differential effects on Akt activation. Whereas EGF treatment of HCC3 and CBO12C3 cells resulted in the phosphorylation of EGFR, Akt, and ERK1/2, and this was highly susceptible to inhibition of gefitinib. In AD3 cells, gefitinib also inhibited the phosphorylation of EGFR and ERK1/2 in response to EGF, but Akt seemed to be constitutively active in the absence of EGF, and phospho-Akt levels in AD3 cells were less susceptible to the effects of gefitinib. Interestingly, LY294002, a selective inhibitor of PI3K, blocked production of VEGF and CXCL1 in HCC3, but not that in AD3, whereas U0126, an ERK1/2 inhibitor, did not have this selective inhibitory effect. Taken together, these different effects of gefitinib on the induction of angiogenesis and the production of angiogenic factors suggest an important role for the Akt pathway. However, as ERK1/2 and PI3K inhibitors also reduced the production of angiogenic factors, these signaling pathways may also play a role in the antiangiogenic effects of gefitinib.

Recent studies have shown that a mutation in exons 18 to 21 of the *EGFR* gene is closely associated with a clinical response to gefitinib in NSCLC patients (18, 19) and that the proliferation of NSCLC cells carrying such EGFR mutations is highly sensitive to gefitinib *in vitro* (18). We, however, could not observe any mutation in exons 18 to 21 of the *EGFR* gene in three lines used in this study (data not shown). Cappuzzo et al. (22) have reported that *EGFR* gene amplification and increased copy number are important to limit therapeutic efficacy of gefitinib in lung cancer. However, there was no difference in gene amplification and copy number of *EGFR* in both HCC3 and AD3 cells. Therefore, altered expression of angiogenic factors and Akt activations between two lines might not be directly associated with gene amplification of *EGFR*.

In this study, AD3 cells showed both constitutive Akt activation and reduced levels of PTEN compared with HCC3 and CBO12C3 cells (Figs. 3*B* and 5*A*). It has been shown that phospho-Akt was recognized as a risk factor for early disease recurrence and poor prognosis of HCC (49). We have previously reported that sensitivity to gefitinib in NSCLC cell lines is associated with EGFR signaling pathways involving Akt and ERK1/2 and is closely linked with cell growth and apoptosis; activation of Akt and/or ERK1/2 was most susceptible to inhibition by gefitinib in one of the nine NSCLC cell lines, which carries a mutation in the EGFR catalytic domain (20). Both PI3K and PTEN are closely associated with activation of Akt, and reducing PTEN levels might be expected to change both Akt activation in response to EGF and its

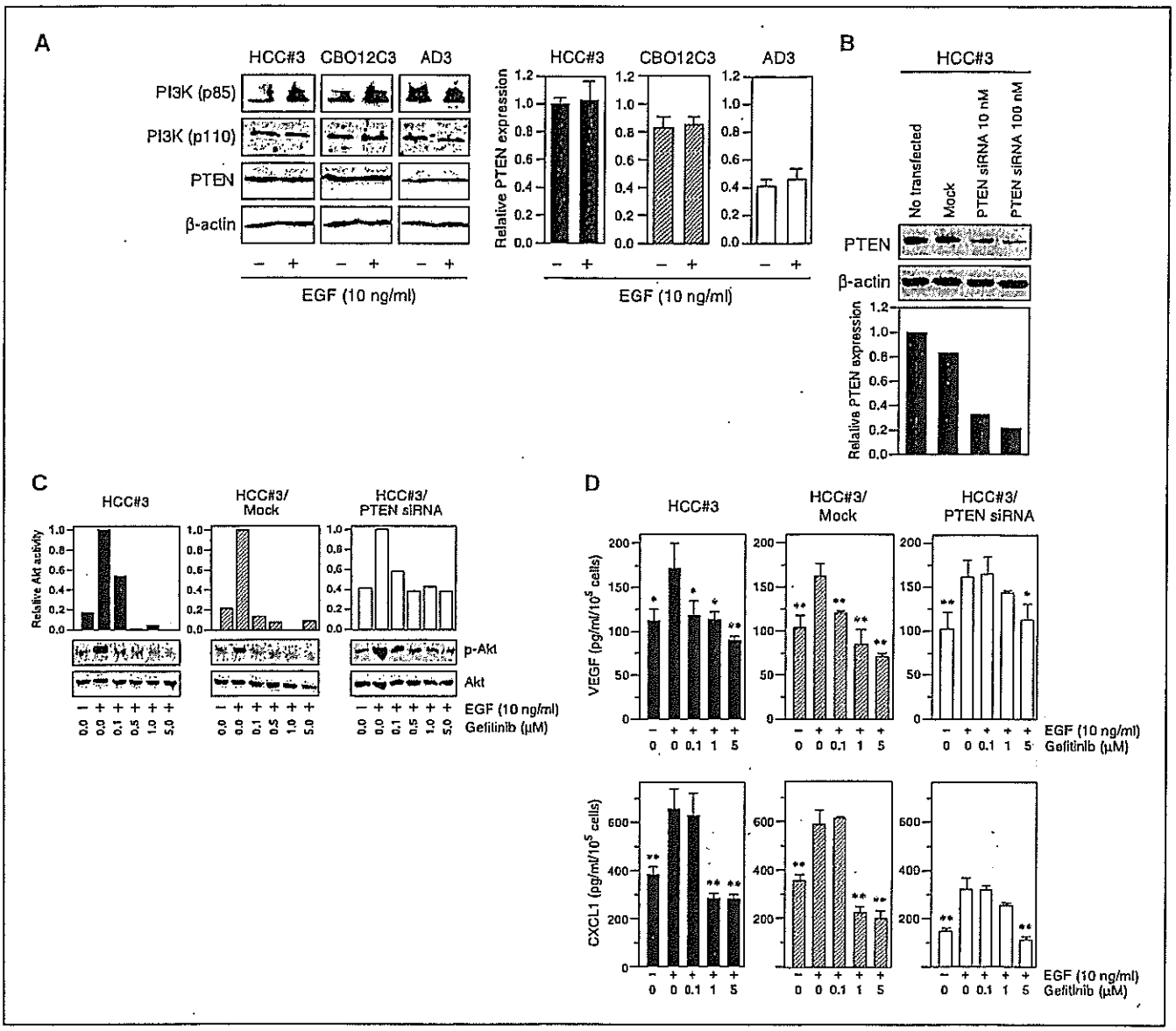

Figure 5. Comparison of PI3K and PTEN protein levels in three HCC cells lines and effects of depleting PTEN using siRNA in HCC3. *A*, HCC cells were cultured with or without 10 ng/mL EGF for 24 hours. Protein extracts were resolved by Western blot analysis with anti-PI3K p110, anti-PTEN, or anti-β-actin antibodies. Levels of PTEN expression were measured by densitometry and normalized to the β-actin levels in each cell line. *Columns*, mean of triplicate experiments; *bars*, SD. *B*, HCC3 cells were transfected with PTEN siRNA, and after 24 hours PTEN levels were determined by Western blot analysis. Levels of PTEN expression were normalized to β-actin levels in each cell line. *C*, effect of PTEN siRNA on Akt phosphorylation in HCC3. Twenty-four hours after transfection with siRNA (100 nmol/L), HCC3 cells were stimulated with 10 ng/mL EGF for 15 minutes, with or without gefitinib at the concentrations indicated. Phosphorylated Akt levels were normalized to nonphosphorylated Akt levels in the presence of EGF but without gefitinib. *D*, effect of PTEN siRNA on inhibition of the EGF-induced production of VEGF and CXCL1 by gefitinib in HCC3. Cells (2.5×10^4/well) were incubated in the presence or absence of 10 ng/mL EGF with or without different doses of gefitinib in 24-well plates for 24 hours. *Columns*, mean of triplicate wells for nontransfected (*closed*), mock-transfected (*hatched*), and PTEN siRNA-transfected cells (*open*); *bars*, SD. *, $P < 0.05$; **, $P < 0.01$ compared with treatment with EGF alone using the two-tailed Student's *t* test.

sensitivity to gefitinib. Reducing *PTEN* gene expression in HCC3 cells using PTEN siRNA indeed decreased the sensitivity of both Akt activation and the production of VEGF and CXCL1 to gefitinib (Fig. 5). Another study has shown that loss of PTEN expression contributed to resistance to gefitinib by permitting Akt activation independently of receptor kinase signaling, in EGFR-expressing tumor cells (50). These findings support our current evidence for a role of constitutive Akt activation in the gefitinib resistance shown by angiogenesis induced by AD3 cells. However, further studies will be required to understand exactly how constitutive Akt activation is associated with the sensitivity or resistance of EGFR signaling to gefitinib.

Acknowledgments

Received 10/12/2005; revised 2/15/2006; accepted 3/16/2006.

Grant support: Ministry of Education Culture, Sports Science, and Technology of Japan (M. Ono and M. Kuwano) and the Second Comprehensive 10-Year Strategy for Cancer Control from the Ministry of Health, Welfare and Labor (M. Kuwano).

The costs of publication of this article were defrayed in part by the payment of page charges. This article must therefore be hereby marked *advertisement* in accordance with 18 U.S.C. Section 1734 solely to indicate this fact.

We thank Naomi Shinbaru (Kyushu University) for editorial help.

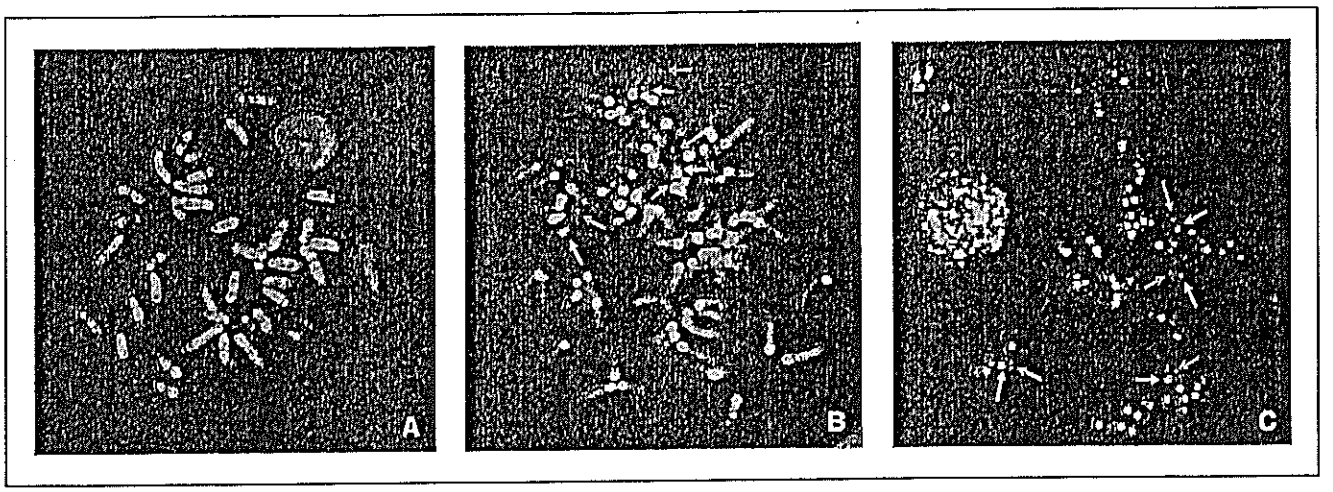

Figure 6. Detection of gene amplification and copy number of *EGFR* gene in HCC3 and AD3 cells by FISH analysis. The digoxigenin-labeled EGFR and biotin-labeled chromosome 11 probes were detected using antidigoxigenin-Cy3 (*yellow*) and anti-biotin-Cy5 (*red*). Representative metaphase spreads from normal spleen cells (*A*), HCC3 cells (*B*), and AD3 cells (*C*). The hybridized probe was detected by fluorescence microscopy.

References

1. Llovet JM, Burroughs A, Bruix J. Hepatocellular carcinoma. Lancet 2003;362:1907–17.
2. Hisaka T, Yano H, Haramaki M, Utsunomiya I, Kojiro M. Expressions of epidermal growth factor family and its receptor in hepatocellular carcinoma cell lines: relationship to cell proliferation. Int J Oncol 1999;14: 453–60.
3. Cross M, Dexter TM. Growth factors in development, transformation, and tumorigenesis. Cell 1991;64:271–80.
4. Wells A. Tumor invasion: role of growth factor-induced cell motility. Adv Cancer Res 2000;78:31–101.
5. Olayioye MA. Update on HER-2 as a target for cancer therapy: intracellular signaling pathways of ErbB2/HER-2 and family members. Breast Cancer Res 2001;3:385–9.
6. Prenzel N, Fischer OM, Streit S, Hart S, Ullrich A. The epidermal growth factor receptor family as a central element for cellular signal transduction and diversification. Endocr Relat Cancer 2001;8:11–31.
7. Iihara K, Shiozaki H, Tahara H, et al. Prognostic significance of transforming growth factor-α in human esophageal carcinoma. Implication for the autocrine proliferation. Cancer 1993;71:2902–29.
8. Hu G, Liu W, Mendelsohn J, et al. Expression of epidermal growth factor receptor and human papilloma virus E6/E7 proteins in cervical carcinoma cells. J Natl Cancer Inst 1997;89:1271–6.
9. Grandis JR, Zeng Q, Drenning SD, Tweardy DJ. Normalization of EGFR mRNA levels following restoration of wild-type p53 in a head and neck squamous cell carcinoma cell line. Int J Oncol 1998;13:375–8.
10. Woodburn JR. The epidermal growth factor receptor and its inhibition in cancer therapy. Pharmacol Ther 1999;82:241–50.
11. Albanell J, Rojo F, Baselga J. Pharmacodynamic studies with the epidermal growth factor receptor tyrosine kinase inhibitor ZD1839. Semin Oncol 2001;28: 56–66.
12. Ciardiello F, Caputo R, Bianco R, et al. Antitumor effect and potentiation of cytotoxic drugs activity in human cancer cells by ZD-1839 (Iressa), an epidermal growth factor receptor-selective tyrosine kinase inhibitor. Clin Cancer Res 2000;6:2053–63.
13. Sirotnak FM, Zakowaski MF, Miller VA, Scher HI, Kris MD. Efficacy of cytotoxic agents against human tumor xenografts is markedly enhanced by coadministration of ZD1839 (Iressa), an inhibitor of EGFR tyrosine kinase. Clin Cancer Res 2000;6:4885–92.
14. Kris MG, Tonato M. New approaches in the treatment of non-small cell lung cancer: taxanes in the treatment of NSCLC: pathway to progress. Lung Cancer 2002;38:1–3.
15. Fukuoka M, Yano S, Giaccone G, et al. Multi-institutional randomized phase II trial of gefitinib for previously treated patients with advanced non-small-cell lung cancer. J Clin Oncol 2003;21:2237–46.
16. Kris MG, Natale RB, Herbst RS, et al. Efficacy of gefitinib, an inhibitor of the epidermal growth factor receptor tyrosine kinase, in symptomatic patients with non-small cell lung cancer: a randomized trial. JAMA 2003;290:2149–58.
17. Ranson M. ZD1839 (Iressa): for more than just non-small cell lung cancer. Oncologist 2002;7:16–24.
18. Paez JG, Janne PA, Lee JC, et al. EGFR mutations in lung cancer: correlation with clinical response to gefitinib therapy. Science 2004;304:1497–500.
19. Lynch TJ, Bell DW, Sordella R, et al. Activating mutations in the epidermal growth factor receptor underlying responsiveness of non-small-cell lung cancer to gefitinib. N Engl J Med 2004;350:2129–39.
20. Ono M, Hirata A, Kometani T, et al. Sensitivity to gefitinib (Iressa, ZD1839) in non-small cell lung cancer cell lines correlates with dependence on the epidermal growth factor (EGF) receptor/extracellular signal-regulated kinase 1/2 and EGF receptor/Akt pathway for proliferation. Mol Cancer Ther 2004;3:465–72.
21. Cappuzzo F, Magrini E, Ceresoli GL, et al. Akt phosphorylation and gefitinib efficacy in patients with advanced non-small-cell lung cancer. J Natl Cancer Inst 2004;4:1133–41.
22. Cappuzzo F, Hirsch FR, Rossi E, et al. Epidermal growth factor receptor gene and protein and gefitinib sensitivity in non-small-cell lung cancer. J Natl Cancer Inst 2005;97:643–55.
23. Moroni M, Veronese S, Benvenuti S, et al. Gene copy number for epidermal growth factor receptor (EGFR) and clinical response to anti-EGFR treatment in colorectal cancer: a cohort study. Lancet Oncol 2005;6: 279–86.
24. Tanigawa N, Lu C, Mitsui T, Miura S. Quantitation of sinusoid-like vessels in hepatocellular carcinoma: its clinical and prognostic significance. Hepatology 1997;26: 1216–23.
25. Folkman J. What is the evidence that tumors are angiogenesis dependent? J Natl Cancer Inst 1990;82:4–6.
26. Kawahara N, Ono M, Taguchi K, et al. Enhanced expression of thrombospondin-1 and hypovascularity in human cholangio carcinoma. Hepatology 1998;28:1512–7.
27. Poon RT, Lau CP, Ho JW, Yu WC, Fan ST, Wong J. Tissue factor expression correlates with tumor angiogenesis and invasiveness in human hepatocellular carcinoma. Clin Cancer Res 2003;9:5339–45.
28. Akiba J, Yano H, Ogasawara S, Higaki K, Kojiro M. Expression and function of interleukin-8 in human hepatocellular carcinoma. Int J Oncol 2001;18:257–64.
29. Iguchi A, Kitajima I, Yamakuchi M, et al. PEA3 and AP-1 are required for constitutive IL-8 gene expression in hepatoma cells. Biochem Biophys Res Commun 2000; 279:166–71.
30. Ren Y, Tsui HT, Poon RT, et al. Macrophage migration inhibitory factor: roles in regulating tumor cell migration and expression of angiogenic factors in hepatocellular carcinoma. Int J Cancer 2003;107:22–9.
31. Sugano Y, Matsuzaki K, Tahashi Y, et al. Distortion of autocrine transforming growth factor β signal accelerates malignant potential by enhancing cell growth as well as PAI-1 and VEGF production in human hepatocellular carcinoma cells. Oncogene 2003;22: 2309–21.
32. Ogasawara S, Yano H, Higaki K, et al. Expression of angiogenic factors, basic fibroblast growth factor and vascular endothelial growth factor, in human biliary tract carcinoma cell lines. Hepatol Res 2001;20:97–113.
33. Ren Y, Poon RT, Tsui HT, et al. Interleukin-8 serum levels in patients with hepatocellular carcinoma: correlations with clinicopathological features and prognosis. Clin Cancer Res 2003;9:5996–6001.
34. Ishikawa H, Nakao K, Matsumoto K, et al. Anti-angiogenic gene therapy for hepatocellular carcinoma using angiostatin gene. Hepatology 2003;37:696–704.
35. Liu Y, Poon RT, Li Q, Kok TW, Lau C, Fan ST. Both antiangiogenesis- and angiogenesis-independent effects are responsible for hepatocellular carcinoma growth arrest by tyrosine kinase inhibitor PTK787/ZK222584. Cancer Res 2005;65:3691–9.
36. Hirata A, Ogawa S, Kometani T, et al. ZD1839 (Iressa) induces antiangiogenic effects through inhibition of epidermal growth factor receptor tyrosine kinase. Cancer Res 2002;62:2554–60.
37. Hirata A, Uehara H, Izumi K, Naito S, Kuwano M, Ono M. Direct inhibition of EGF receptor activation in vascular endothelial cells by gefitinib ("Iressa", ZD1839). Cancer Sci 2004;7:614–8.
38. Ito Y, Takeda T, Sakon M, et al. Expression and clinical significance of erb-B receptor family in hepatocellular carcinoma. Br J Cancer 2001;84:1377–83.
39. Kadohama T, Tsuji K, Ogawa K. Indistinct cell cycle checkpoint after UV damage in H-ras-transformed

mouse liver cells despite normal p53 gene expression. Oncogene 1994;9:2845–52.
40. Yoshie M, Nishimori H, Lee GH, Ogawa K. High colony forming capacity of primary cultures hepatocytes as a dominant trait in hepatocarcinogenesis-susceptible and resistant mouse strains. Carcinogenesis 1998;19: 1103–7.
41. Ono M, Kawahara N, Goto D, et al. Inhibition of tumor growth and neovascularization by an anti-gastric ulcer agent, irsogladine. Cancer Res 1996;56:1512–6.
42. Yarden Y. The EGFR family and its ligands in human cancer signalling mechanisms and therapeutic opportunities. Eur J Cancer 2001;37:3–8.
43. Henegariu O, Artan S, Greally JM, et al. Cryptic translocation identification in human and mouse using several telomeric multiplex fish (TM-FISH) strategies. Lab Invest 2001;81:483–91.
44. Maehama T, Dixon JE. The tumor suppressor, PTEN/MMAC1, dephosphorylates the lipid second messenger, phosphatidylinositol 3,4,5-trisphosphate. J Biol Chem 1998;273:13375–8.
45. Ciardiello F, Bianco R, Damiano V, et al. Antiangiogenic and antitumor activity of anti-epidermal growth factor receptor C225 monoclonal antibody in combination with vascular endothelial growth factor antisense oligonucleotide in human GEO colon cancer cells. Clin Cancer Res 2000;6:3739–47.
46. Petit AM, Rak J, Hung MC, et al. Neutralizing antibodies against epidermal growth factor and ErbB-2/neu receptor tyrosine kinases down-regulate vascular endothelial growth factor production by tumor cells *in vitro* and *in vivo*: angiogenic implications for signal transduction therapy of solid tumors. Am J Pathol 1997; 151:1523–30.
47. Ryuto M, Ono M, Izumi H, et al. Induction of vascular endothelial growth factor by tumor necrosis factor α in human glioma cells. Possible roles of SP-1. J Biol Chem 1996;271:28220–8.
48. Yoshida S, Ono M, Shono T, et al. Involvement of interleukin-8, vascular endothelial growth factor, and basic fibroblast growth factor in tumor necrosis factor α-dependent angiogenesis. Mol Cell Biol 1997; 17:4015–23.
49. Nakanishi K, Sakamoto M, Yamasaki S, Todo S, Hirohashi S. Akt phosphorylation is a risk factor for early disease recurrence and poor prognosis in hepatocellular carcinoma. Cancer 2005;103:307–12.
50. Bianco R, Shin I, Ritter CA, et al. Loss of PTEN/MMAC1/TEP in EGF receptor-expressing tumor cells counteracts the antitumor action of EGFR tyrosine kinase inhibitors. Oncogene 2003;22:2812–22.

17β-Estradiol Induces Down-Regulation of *Cap43/NDRG1/Drg-1*, a Putative Differentiation-Related and Metastasis Suppressor Gene, in Human Breast Cancer Cells

Abbas Fotovati,[1] Teruhiko Fujii,[1,2] Miki Yamaguchi,[1,2] Masayoshi Kage,[3] Kazuo Shirouzu,[2] Shinji Oie,[4] Yuji Basaki,[4] Mayumi Ono,[4,5] Hideaki Yamana,[1] and Michihiko Kuwano[1]

Abstract **Purpose:** Cap43 is known as a nickel- and calcium-inducible gene. In the present study, we examined whether 17β-estradiol (E_2) could affect the expression of Cap43 in breast cancer.

Experimental Design: Real-time PCR, immunoblotting, and immunocytochemistry were used to examine the expression of Cap43 and estrogen receptor-α (ER-α) in breast cancer cell lines. MDA-MB-231 and SK-BR-3 cell lines were transfected with ER-α cDNA to establish cells overexpressing ER-α. Immunohistochemistry was used to evaluate the expression of the Cap43 protein in breast cancer patients ($n = 96$), and the relationship between Cap43 expression and clinicopathologic findings was examined.

Results: Of the eight cell lines, four expressed higher levels of Cap43 with very low levels of ER-α, whereas the other four expressed lower levels of Cap43 with high ER-α levels. Treatment with E_2 decreased the expression of Cap43 dose dependently in ER-α–positive cell lines but not in ER-α–negative lines. Administration of antiestrogens, tamoxifen and ICI 182780, abrogated the E_2-induced down-regulation of Cap43. Overexpression of ER-α in both ER-α–negative cell lines, SK-BR-3 and MDA-MB-231, resulted in down-regulation of Cap43. Immunostaining studies showed a significant correlation between Cap43 expression and the histologic grade of tumors ($P = 0.0387$). Furthermore, Cap43 expression was inversely correlated with the expression of ER-α ($P = 0.0374$).

Conclusions: E_2-induced down-regulation of Cap43 seems to be mediated through ER-α–dependent pathways in breast cancer cells both in culture and in patients. Cap43 has potential as a molecular marker to determine the therapeutic efficacy of antiestrogenic anticancer agents in breast cancer.

Cap43 has been identified as a nickel- and calcium-inducible gene (1). The Cap43, a 43-kDa protein, has three unique 10–amino acid tandem-repeat sequences at its carboxyl terminus and is phosphorylated by protein kinase A (2). The *Cap43* gene is identical to the N-myc downstream regulated gene 1 (*NDRG1*), a human homocysteine-inducible gene (3), and to the differentiation-related gene-1 (4). Cap43 expression is reduced in tumor cells (*RTP/Rit42*; ref. 5). Furthermore, the expression of Cap43 is markedly influenced by several stimuli, including oxidative stress, metal ions, hypoxia, phorbol esters, vitamins A and D, steroids, homocysteine, and tunicamycin as well as oncogenes (*N-myc* and *C-myc*) and tumor suppressor genes (p53 and VHL; refs. 1, 3, 5–10).

Although several studies have elucidated various characteristics of the Cap43, its exact function remains unclear. Cap43 is expressed in various organs, including the prostate, ovary, colon, and kidney, and its expression is dynamically changed during postnatal development in the kidney, brain, liver, and nerves (3, 11–13). These studies, which suggest the involvement of Cap43 in organ maturation and differentiation, have recently prompted detailed investigations of its role in the neuronal system. Cap43 was originally shown to be responsible for Charcot-Marie-Tooth disease type 4D; mutations in *Cap43* are commonly identified in this hereditary neuropathy of the motor and sensory systems. Okuda et al. have recently established Cap43 knockout mice that exhibit Schwann cell dysfunction, suggesting that Cap43 is essential for the maintenance of the myelin sheaths in peripheral nerves (14). Consistent with this study, Hirata et al. have reported that Cap43 plays an important role in the terminal differential of Schwann cells during nerve regeneration (15).

In contrast with these studies, Stein et al. have identified *Cap43* as a gene that is up-regulated by p53 and have also

Authors' Affiliations: [1]Center for Innovative Cancer Therapy of the 21st Century Center of Excellence Program for Medical Science and Departments of [2]Surgery and [3]Pathology, Kurume University, Kurume, Japan and [4]Station-II for Collaborative Research and [5]Department of Medical Biochemistry, Graduate School of Medical Sciences, Kyushu University, Fukuoka, Japan

Received 9/7/05; revised 3/4/06; accepted 3/10/06.

Grant support: Ministry of Health, Welfare and Labor of Japan Third-Term Comprehensive 10-Year Strategy for Cancer Control grant-in-aid and Kurume University 21st Century Center of Excellence Program for Medical Science.

The costs of publication of this article were defrayed in part by the payment of page charges. This article must therefore be hereby marked *advertisement* in accordance with 18 U.S.C. Section 1734 solely to indicate this fact.

Requests for reprints: Teruhiko Fujii, Center for Innovative Cancer Therapy of the 21st Century Center of Excellence Program for Medical Science, Kurume University, 67 Asahi-machi, Kurume, Fukuoka 830-0011, Japan. Phone: 81-942-31-7748; Fax: 81-942-31-7749; E-mail: tfujii@med.kurume-u.ac.jp.

doi:10.1158/1078-0432.CCR-05-1962

shown that Cap43 is required for p53-dependent apoptosis, thereby indicating that *Cap43* is a p53 target gene (16). Furthermore, Kim et al. have reported that the Cap43 is associated with microtubules in the centrosome and participates in the spindle checkpoint in a p53-dependent manner, suggesting that Cap43 may play a key role in the regulation of microtubule dynamics (17). Overexpression of the *Cap43* gene also inhibits growth in colon cancers as well as metastasis in prostate and colon cancer cells in an animal model (18, 19), suggesting that Cap43 suppresses metastasis. Low levels of Cap43 expression in breast cancer cells are closely correlated with poor clinical outcomes (20). Cap43 thus seems to be closely associated with the differentiation and/or malignant states of human cancers.

In the present study, we examine how the expression of the *Cap43* gene could be modulated during therapeutic treatment by antiestrogenic drugs and discuss the potential of Cap43 as a molecular target for the therapeutic efficacy of antiestrogenic anticancer agents in breast cancer.

Materials and Methods

Cells and cell culture. Human breast cancer cells SK-BR-3, MDA-MB-231, T47D, MCF-7, and CRL1500 were obtained from the American Type Culture Collection (Manassas, VA). YMB-1 and OCUB-M were obtained from the Japanese Collection of Research Bioresources (Osaka, Japan) and Riken/Wako (Osaka, Japan), respectively. A tamoxifen-resistant cell line, R-27, was established from MCF-7 (21). All cell lines were grown in phenol red–free McCoy's (PromoCell GmbH, Heidelberg, Germany) and Leibovitz's L-15, RPMI 1640, and α-MEM containing 10% fetal bovine serum, 100 units/mL penicillin G sodium, and 100 μg/mL streptomycin sulfate.

Estrogen receptor-α overexpression in estrogen receptor–negative cell lines. Two estrogen receptor-α (ER-α)–negative cell lines, SK-BR-3 and MDA-MB-231, were transfected with either pRc/CMV vector or ER-α plasmid DNA (a kind gift from Dr. Shin-ichi Hayashi, Department of Molecular Medical Technology, Faculty of Medicine, Tohoku University, Sendai, Japan) using LipofectAMINE Plus (Invitrogen Life Technologies, Inc., Gaithersburg, MD). Three days after transfection, 500 μg/mL G418 disulfate (Nacalai Tesque, Kyoto, Japan) was added to the growth medium. The resulting G418-resistant cells were propagated to generate stable cell lines for use in further studies.

Cell proliferation assay. Cells were plated at 2×10^4 per well in 12-well dishes. After 48 hours, cells were rinsed and incubated for a further 24 hours in same medium supplemented with 5% double charcoal-stripped serum CSS. Cells were then washed with serum-, estrogen-, and phenol red–free medium and then incubated in medium supplemented with 5% CSS in the presence or absence of 17β-estradiol E_2 (Sigma-Aldrich Co., St. Louis, MO) with or without tamoxifen (Calbiochem, La Jolla, CA). The cells were trypsinized and counted at 0, 2, 4, and 6 days after incubation with a coulter counter (Beckman Coulter, Miami, FL).

Immunocytochemistry. Cells were trypsinized and plated on glass coverslips in six-well plates. Then, cells were rinsed with PBS and fixed in 4% paraformaldehyde/PBS for 30 minutes at room temperature. Cells were permeabilized with solution containing 5% bovine serum albumin, 0.2% Triton X-100 in PBS for 90 minutes at room temperature. After 1 hour of blocking with 2% goat serum, the cells were incubated ovemight with rabbit polyclonal anti-Cap43 (1:1,000; developed in our laboratory; ref. 10). Cells were then rinsed and incubated with goat anti-rabbit IgG and 1 μg/mL Alexa Fluor 546 (Molecular Probes, Eugene, OR) for 60 minutes at room temperature. Nuclear staining was carried out using 4′,6-diamidino-2-phenylindole (1:1,000, Dojindo, Kumamoto, Japan). Coverslips were mounted on slide glasses using gel mount and viewed using an Olympus BX51 florescence microscope (Olympus, Tokyo, Japan).

Western blot analysis. After treatment with E_2, tamoxifen, ICI 182780 (Nacalai Tesque), or nickel chloride ($NiCl_2$; Nacalai Tesque), 200 μL lysis buffer [0.2% NP40, 225 mmol/L NaCl, 25 mmol/L Tris (pH 7.4)] was added. The cells were harvested, and the cell slurry was sonicated briefly before centrifugation at 15,000 × *g* for 15 minutes at 4°C. The supematant was collected, and 50 μg aliquots of protein were loaded into each well, separated using SDS-PAGE, and transferred to Immobilon membranes (Millipore, Bedford, MA). After transfer, blots were incubated with blocking solution and probed with antibodies. The antibodies used were as follows: rabbit polyclonal antibody directed against Cap43 (produced in our laboratory; ref. 10), rabbit polyclonal anti-ER-α antibody (Santa Cruz Biotechnology, Inc., Santa Cruz, CA), and anti-β-actin (Sigma-Aldrich). The relative expression of each protein was calculated using the NIH Image Analysis Program version 1.62 (NIH, Bethesda, MD).

RNA extraction and cDNA synthesis. Total RNA was extracted using ISOGEN-LS reagent (Nippon Gene, Toyama, Japan) and digested with DNase I (Sigma-Aldrich). Total RNA (1 μg) was then reverse transcribed using random hexamer priming and SuperScript II reverse transcriptase (Toyobo, Osaka, Japan).

Real-time PCR. cDNA (100 ng) was amplified in a real-time PCR using SYBR Green Mix (PE Applied Biosystems, Warrington, United Kingdom) and 200 nmol/L primer for Cap43. The real-time PCR reactions were done in an ABI PRISM Model 7700 Sequence Detector (Applied Biosystems, Foster City, CA) under the following conditions: 50°C for 2 minutes, 95°C for 1 minute followed by 40 cycles at 95°C for 15 seconds and 60°C for 1 minute. The sequences of primers were as follows: *Cap43* forward primer 5′-AGGCGGACATTCTGGAAATG-3′ and reverse primer 5′-CGGTACTTCCCCAGCACACTT-3′, *pS2* forward primer 5′-TTTGGAGCAGAGAGGAGGCAATGG-3′ and reverse primer 5′-TGGTATTAGGATAGAAGCACCAGGG-3′, and *C-myc* forward primer 5′-AGGCGCGCGTAGTTAATTCAT-3′ and reverse primer 5′-CGCCC-TCTGCTTTGGGA-3′. Glyceraldehyde-3-phosphate dehydrogenase and β-actin were used as reference genes.

Immunohistochemistry. Tissue sections were taken from 96 breast cancer patients who underwent radical surgery (Department of Surgery, Kurume University Hospital, Kurume, Japan) between 1995 and 1999. The 4-μm tissue sections were deparaffinized for 15 minutes at 85°C and the slides were heated in a microwave oven in a CC1 buffer for 60 minutes. The sections were stained using the Benchmark (IHC Automated Systems, Tucson, AZ) with rabbit polyclonal anti-Cap43 (9, 10), anti-ER-α, anti–progesterone receptor (PgR), anti–epidermal growth factor receptor (EGFR), and anti-HER-2 antibody. All antibodies else than Cap43 (produced in our laboratory) were purchased from Ventana Medical Systems (Tucson, AZ). The samples were viewed using an Olympus BX51 florescence microscope.

The extent to which Cap43 proteins were stained in immunohistologic studies was analyzed to compare the strength of Cap43 expression in cancer cells with that in normal glands: cancer cells that expressed Cap43 stronger than normal glands appeared positive for staining and normal glands expressing Cap43 stronger than cancer cells were negative for staining. The extent to which ER-α or PgR proteins were stained in immunohistologic studies was defined by the percentage of cells with strongly stained nuclei: ≥10% defined a gland as positive for ER-α or PgR and ≤9% defined it as negative. The immunohistochemical expression of EGFR and HER-2 was categorized into four groups: score 0, no staining at all or membrane staining in <10% of the tumor cells; score 1+, faint/barely perceptible partial membrane staining in >10% of the tumor cells; score 2+, weak to moderate staining of the entire membrane in >10% of the tumor cells; score 3+, strong staining of the entire membrane in >10% of the tumor cells. The extent of immunohistologic staining for EGFR and HER-2 was defined as follows: scores of 2+ or 3+ were regarded as positive and scores of 0 or 1+ were regarded as negative. The positive cells were counted by two experienced observers who were blinded to the condition of the

patients. The relationship between Cap43 and each clinicopathologic finding (age, tumor size, menopausal status, histologic grade, lymph node metastasis, and expression of EGFR, HER-2, ER-α, and PgR) and postoperative survival was examined.

Statistical analysis. The χ^2 test, Fisher's exact probability test, and Student's t test were used for statistical analyses. In patients undergoing resection, the relationships between Cap43 expression and prognosis were examined by the Kaplan-Meier method (22) and the univariate relationship between prognostic factors and overall survival rate was assessed by the log-rank test. $P < 0.05$ was regarded as statistically significant.

Results

Comparison of cellular levels of Cap43 and ER-α in human breast cancer. All eight breast cancer cell lines used in this study were screened for Cap43 expression using immunoblotting and Immunocytochemistry (Fig. 1). SK-BR-3, MDA-MB-231, CRL1500, OCUB-M, and R-27 showed relatively high levels of Cap43 protein expression, whereas its expression was decreased in T47D, MCF-7, and YMB-1 (Fig. 1A). ER-α was expressed in T47D, MCF-7, YMB-1, and R-27, but its expression was negligible in SK-BR-3, MDA-MB-231, CRL1500, and OCUB-M. Consistent with the results from Western blot analysis (Fig. 1A), immunocytochemical analysis of the eight cell lines showed the expression of Cap43 in SK-BR-3, MDA-MB-231, CRL1500, OCUB-M, and R-27 (Fig. 1B). A tamoxifen-resistant cell line, R-27, showed a much higher expression of Cap43 protein than its parental counterpart cell line, MCF-7 (Fig. 1A and B). We conducted further studies to examine whether the expression of ER-α in these cell lines, and the addition of E_2, tamoxifen, and ICI 182780, to the culture could modulate the expression of Cap43. Three ER-α-positive (T47D, MCF-7, and R-27) and two ER-α-negative (SK-BR-3 and MDA-MB-231) cell lines were selected for further study.

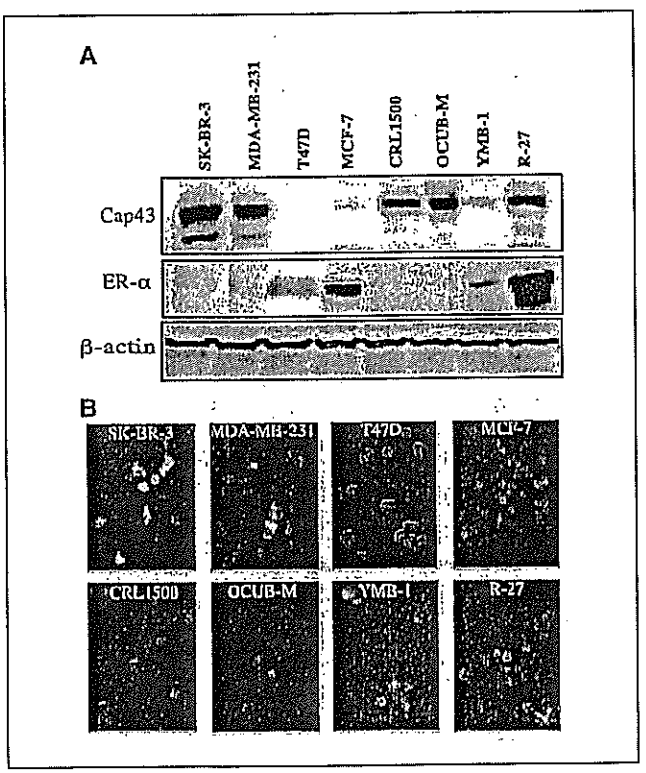

Fig. 1. Protein expression of Cap43 and ER-α in eight breast cancer cell lines. *A*, cellular protein levels of Cap43 and ER-α were determined by Western blot analysis. *B*, cells were viewed using an Olympus BX51 fluorescence microscope and photographed with an Olympus DP-70 digital camera. Magnification, ×200. *Green*, Cap43.

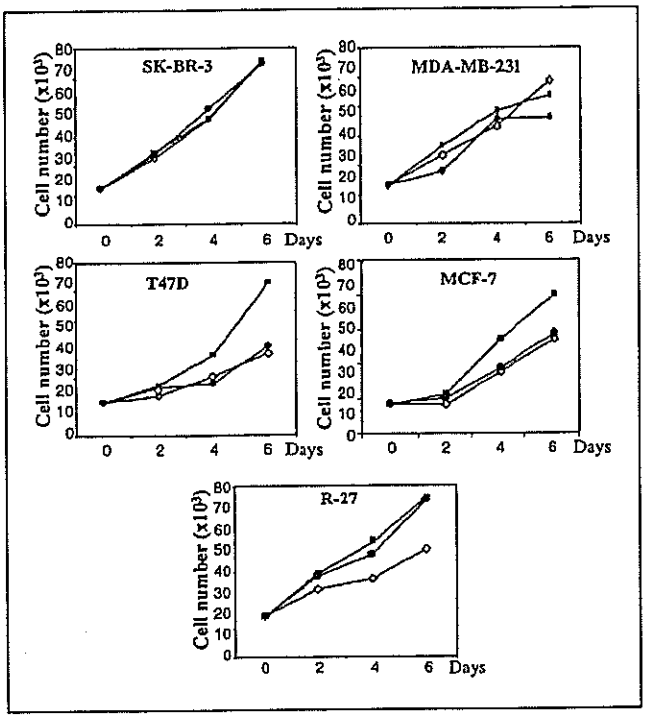

Fig. 2. Effect of E_2 (10^{-9} mol/L) with or without tamoxifen (10^{-6} mol/L) on cell growth. The cells were trypsinized and counted with a Coulter counter at the indicated times. ◇, E_2 (−); ■, E_2 (10^{-8} mol/L); ●, E_2 (10^{-8} mol/L) + tamoxifen (10^{-6} mol/L).

Cell growth dependence on E_2 and the effect of tamoxifen. We used an E_2-depleted culture condition to examine whether the addition of E_2 to the five breast cancer cell lines tested in this experiment promoted E_2-dependent growth. Previous studies have shown that the growth of human breast cancer cell lines depends on the presence of 10^{-8} to 10^{-9} mol/L E_2 in the culture medium (23, 24). Of the five cell lines, the addition of 10^{-8} mol/L E_2 enhanced growth in the ER-α-positive cell lines (T47D, MCF-7, and R-27). However, neither of the ER-α-negative lines, SK-BR-3 and MDA-MB-231, showed enhanced growth on the addition of E_2 to the culture (Fig. 2). Tamoxifen at 10^{-6} mol/L inhibited E_2-induced cell growth in T47D and MCF-7 cell lines, resulting in a degree of growth similar to that observed in the absence of E_2. However, tamoxifen could not inhibit E_2-induced cell growth in R-27 cells (Fig. 2).

Effects of E_2 with or without tamoxifen or ICI 182780 on Cap43 expression. We next used real-time PCR and Western blotting to examine whether E_2 could modulate expression of Cap43 in cultured breast cancer cells. As shown in Fig. 3A, expression of Cap43 mRNA was markedly down-regulated by exogenous addition of E_2 for 24 hours in the ER-α-positive lines, T47D, MCF-7, and R-27, but not in the ER-α-negative lines, SK-BR-3 and MDA-MB-231 (Fig. 3A). Furthermore, E_2 down-regulated expression of Cap43 in a dose-dependent

manner in the three ER-α-positive cell lines. Tamoxifen at 10^{-6} mol/L or ICI 182780 at 10^{-7} mol/L almost completely abrogated the E_2-induced down-regulation of the Cap43 gene in two ER-α-positive lines, T47D and MCF-7, in the presence of various doses of E_2 (10^{-12} to 10^{-6} mol/L). However, the abrogatory effect of tamoxifen was hardly observed in the tamoxifen-resistant R-27 line in comparison with its parental MCF-7 cells (Fig. 3A). ICI 182780 at 10^{-7} mol/L almost

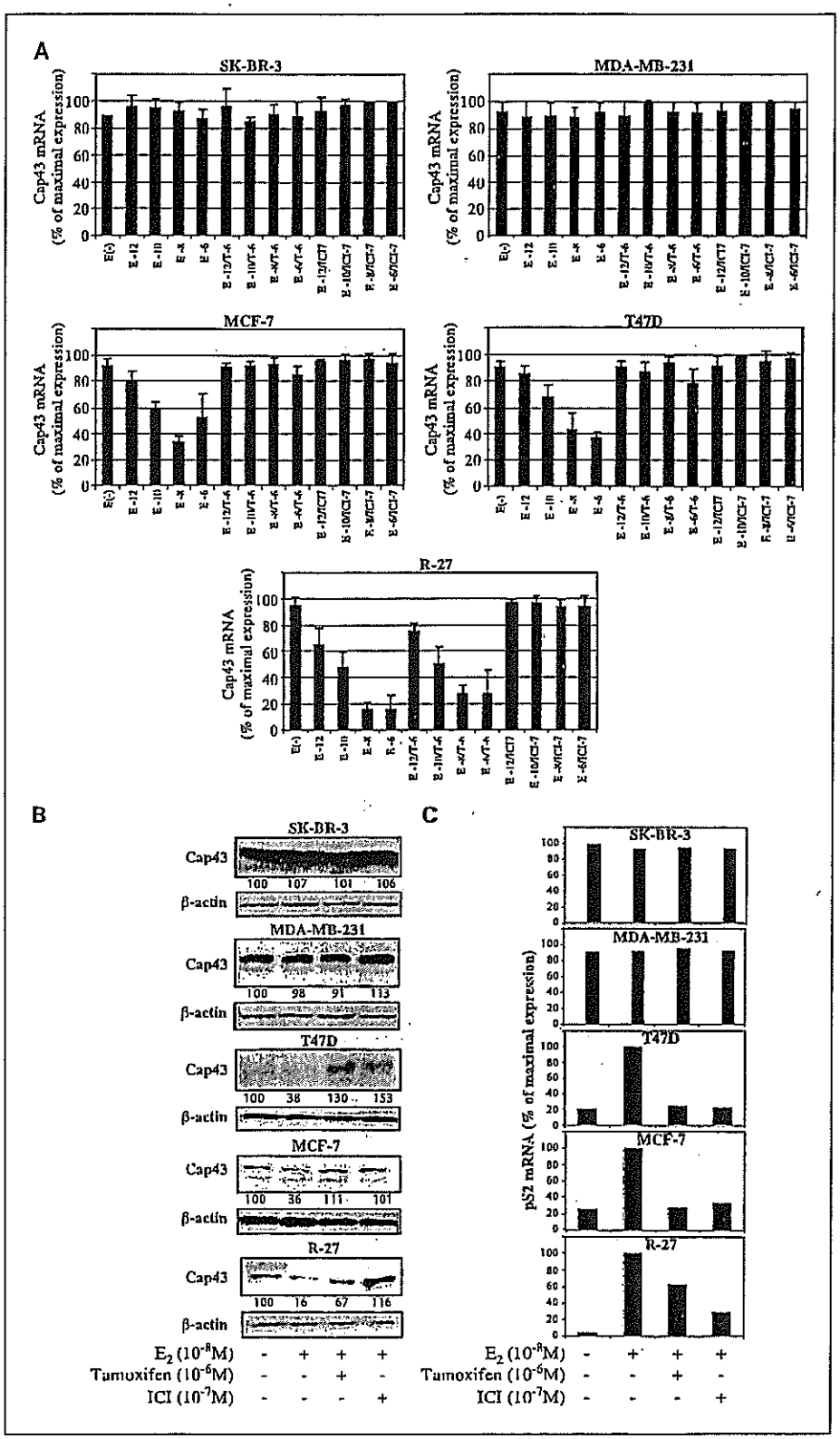

Fig. 3. Effect of E_2 with or without tamoxifen and ICI 182780 on Cap43 expression. *A*, Cap43 mRNA. *E(-)*, E_2 (−); *E-12*, E_2 (10^{-12} mol/L); *E-10*, E_2 (10^{-10} mol/L); *E-8*, E_2 (10^{-8} mol/L); *E-6*, E_2 (10^{-6} mol/L); *E-12/T-6*, E_2 (10^{-12} mol/L) + tamoxifen (10^{-6} mol/L); *E-10/T-6*, E_2 (10^{-10} mol/L) + tamoxifen (10^{-6} mol/L); *E-8/T-6*, E_2 (10^{-8} mol/L) + tamoxifen (10^{-6} mol/L); *E-6/T-6*, E_2 (10^{-6} mol/L) + tamoxifen (10^{-6} mol/L); *E-12/ICI-7*, E_2 (10^{-12} mol/L) + ICI 182780 (10^{-7} mol/L); *E-10/ICI-7*, E_2 (10^{-10} mol/L) + ICI 182780 (10^{-7} mol/L); *E-8/ICI-7*, E_2 (10^{-8} mol/L) + ICI 182780 (10^{-7} mol/L); *E-6/ICI-7*, E_2 (10^{-6} mol/L) + ICI 182780 (10^{-7} mol/L). *B*, Cap43 protein. *Numbers*, density of the Cap43 band for each cell line normalized to the density in the absence of any drug (100%). *C*, effects of E_2 with or without tamoxifen and ICI 182780 on pS2 mRNA expression in breast cancer cells. Maximal expression levels of pS2 mRNA in each cell line are normalized as 100%.

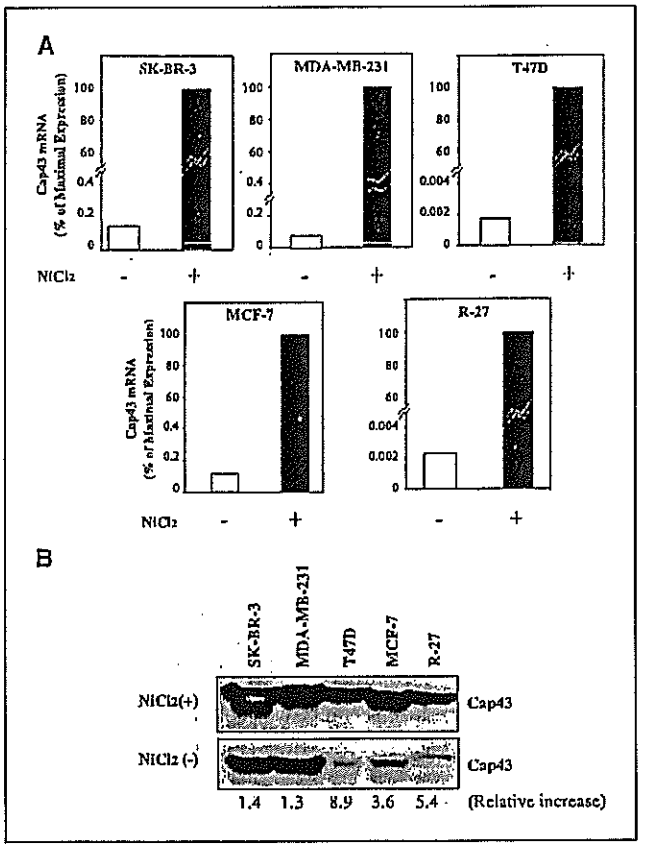

Fig. 4. Enhanced expression of Cap43 gene by nickel in breast cancer cell lines. Expression of Cap43 mRNA (*A*) and Cap43 protein (*B*) were analyzed by real-time PCR and Western blotting, respectively. The relative fold increase of Cap43 protein expression is the amount of Cap43 protein detected in the presence of $NiCl_2$ divided by the amount of Cap43 present in the absence of $NiCl_2$.

completely abrogated the E_2-induced down-regulation of the Cap43 in R-27 cells, whereas tamoxifen at 10^{-6} mol/L could not abrogate the E_2-induced down-regulation of the Cap43 when in the presence of E_2 at 10^{-8} and 10^{-6} mol/L, respectively. In contrast, no marked change in Cap43 mRNA levels in SK-BR-3 and MDA-MB-231 was evident when these cell lines were treated with E_2 in the absence or presence of tamoxifen and ICI 182780 (Fig. 3A). Consistent with the effects on mRNA levels of Cap43, Western blot analysis also showed that the expression of Cap43 protein was decreased in E_2-treated T47D, MCF-7, and R-27 lines and tamoxifen at 10^{-6} mol/L or ICI 182780 at 10^{-7} mol/L abrogated the E_2-induced down-regulation of Cap43 in these three ER-α-positive cell lines. By contrast, neither treatment with E_2 alone nor E_2 with tamoxifen or ICI 182780 affected cellular Cap43 protein levels in the SK-BR-3 or MDA-MB-231 lines (Fig. 3B).

Previous studies have shown that the expression of the *pS2* gene is profoundly affected by E_2 in MCF-7 cells (23–25). The results from the present study are consistent with these findings, showing that administration of E_2 markedly increases expression of pS2 mRNA and that administration of tamoxifen or ICI 182780 blocks this E_2-induced stimulatory effect in the T47D, MCF-7, and R-27 cell lines (Fig. 3C). The inhibitory effect of tamoxifen on the E_2-induced stimulation of pS2 mRNA expression in the R-27 line was much less than that in its parental MCF-7 cells. By contrast, ICI 182780 at 10^{-7} mol/L more greatly abrogated the E_2-induced down-regulation of Cap43 than tamoxifen at 10^{-6} mol/L in R-27 cells. Expression of pS2 mRNA was not affected by either E_2 alone or E_2 and tamoxifen in the SK-BR-3 and MDA-MB-231 (Fig. 3C).

Up-regulation of the Cap43 gene by nickel in all breast cancer cell lines. Cap43 was originally isolated as a gene induced by nickel compounds and its expression is highly susceptible to the presence of nickel (1, 9). We examined whether exposure to nickel at 1 mmol/L for 24 hours could specifically alter the expression of Cap43 in the five breast cancer cell lines. Exposure to nickel markedly enhanced cellular Cap43 mRNA levels in all five lines (Fig. 4A). The marked increase in the levels of Cap43 mRNA seen in these cell lines was observed irrespective of the expression of ER-α (Fig. 4A). Western blot analysis also showed significant increases in the levels of Cap43 protein in nickel-treated cell lines (Fig. 4B). Cap43 protein levels were higher in the two untreated ER-α-negative lines, SK-BR-3 and MDA-MB-231, than in the ER-α-positive lines. However, expression of Cap43 protein was further enhanced in these ER-α-positive cell lines in response to nickel.

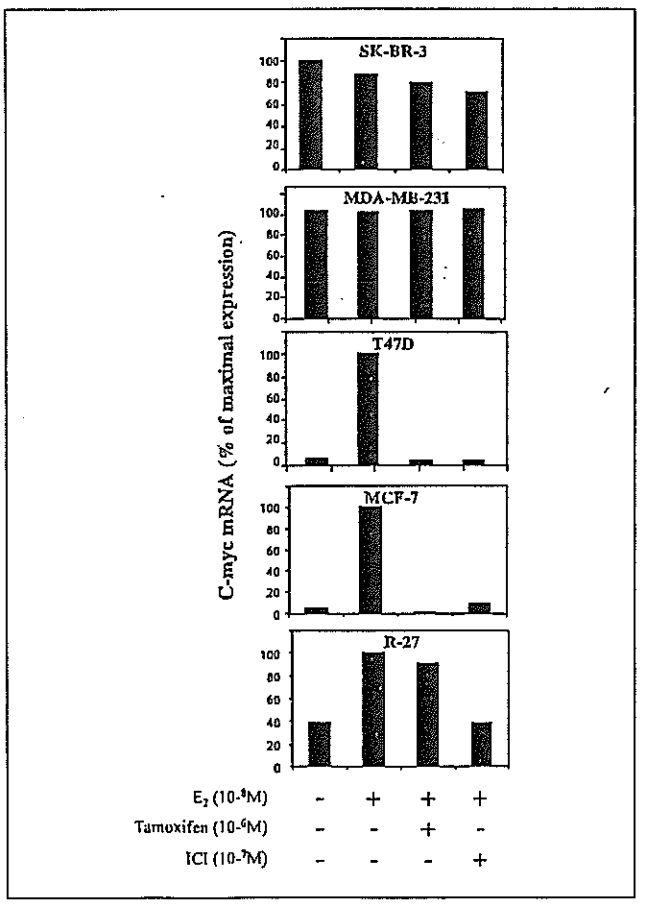

Fig. 5. Effects of E_2 with or without tamoxifen and ICI 182780 on C-myc mRNA expression in breast cancer cell lines. Maximal expression levels of C-myc mRNA in each cell line are normalized as 100%.